Computer Methods and Programs in Biomedicine 215 (2022) 106629

Contents lists available at ScienceDirect

Computer Methods and Programs in Biomedicine

journal homepage: www.elsevier.com/locate/cmpb

A review of image processing methods for fetal head and brain analysis in ultrasound images

Helena R. Torres[a,b,c,d,*], Pedro Morais[d], Bruno Oliveira[a,b,c,d], Cahit Birdir[e,f], Mario Rüdiger[g], Jaime C. Fonseca[a], João L. Vilaça[d]

[a] Algoritmi Center, School of Engineering, University of Minho, Guimarães, Portugal
[b] Life and Health Sciences Research Institute (ICVS), School of Medicine, University of Minho, Braga, Portugal
[c] ICVS/3B's - PT Government Associate Laboratory, Braga/Guimarães, Portugal
[d] 2Ai – School of Technology, IPCA, Barcelos, Portugal
[e] Department of Gynecology and Obstetrics, University Hospital Carl Gustav Carus, TU Dresden, Germany
[f] Saxony Center for Feto-Neonatal Health, TU Dresden, Germany
[g] Department for Neonatology and Pediatric Intensive Care, University Hospital Carl Gustav Carus, TU Dresden, Germany

ARTICLE INFO

Article history:
Received 19 March 2021
Revised 20 December 2021
Accepted 8 January 2022

Keywords:
Brain structures analysis
Anatomical planes
Fetal ultrasound
Head analysis
Neurodevelopment

ABSTRACT

Background and objective: Examination of head shape and brain during the fetal period is paramount to evaluate head growth, predict neurodevelopment, and to diagnose fetal abnormalities. Prenatal ultrasound is the most used imaging modality to perform this evaluation. However, manual interpretation of these images is challenging and thus, image processing methods to aid this task have been proposed in the literature. This article aims to present a review of these state-of-the-art methods.
Methods: In this work, it is intended to analyze and categorize the different image processing methods to evaluate fetal head and brain in ultrasound imaging. For that, a total of 109 articles published since 2010 were analyzed. Different applications are covered in this review, namely analysis of head shape and inner structures of the brain, standard clinical planes identification, fetal development analysis, and methods for image processing enhancement.
Results: For each application, the reviewed techniques are categorized according to their theoretical approach, and the more suitable image processing methods to accurately analyze the head and brain are identified. Furthermore, future research needs are discussed. Finally, topics whose research is lacking in the literature are outlined, along with new fields of applications.
Conclusions: A multitude of image processing methods has been proposed for fetal head and brain analysis. Summarily, techniques from different categories showed their potential to improve clinical practice. Nevertheless, further research must be conducted to potentiate the current methods, especially for 3D imaging analysis and acquisition and for abnormality detection.

1. Introduction

The fetal period is characterized by organ development, providing the basis for subsequent long-term health. Specifically, growth of the head and brain structures in this period determine life-long neurological competencies. Disturbances in head growth and neurodevelopment are associated with long-term health burden, morbidity, and can have an impact on the quality of the infant's life [1]. Thus, the monitoring the growth of head and brain in the fetal period is paramount. Ultrasound (US) imaging has been widely used in prenatal diagnosis for the examination of fetal head and brain. Compared to computed tomography (CT) and magnetic resonance (MR), US imaging presents the advantages of being radiation-free and noninvasive, while providing a real-time and low-cost prenatal examination. Moreover, recent advances in 3D US technology allows the acquisition of 3D volumetric data, enabling a more detailed analysis of the fetus head and central nervous system (CNS) and allowing post-exam data processing [2].

Applications of diagnostic US applied to fetal head/brain include analysis of craniofacial abnormalities or skull deformations [3,4], evaluation of CNS malformations [5,6], fetal biometry analysis [7], assessment of brain development, and gestational age (GA) estimation [8]. These diagnostic applications are frequently performed in 2D images of standard anatomical planes or 3D volumes. For all cases, a robust evaluation of the image is important to extract

* Corresponding author at: 2Ai – School of Technology, IPCA, Barcelos, Portugal.
E-mail address: htorres@ipca.pt (H.R. Torres).

https://doi.org/10.1016/j.cmpb.2022.106629
0169-2607/

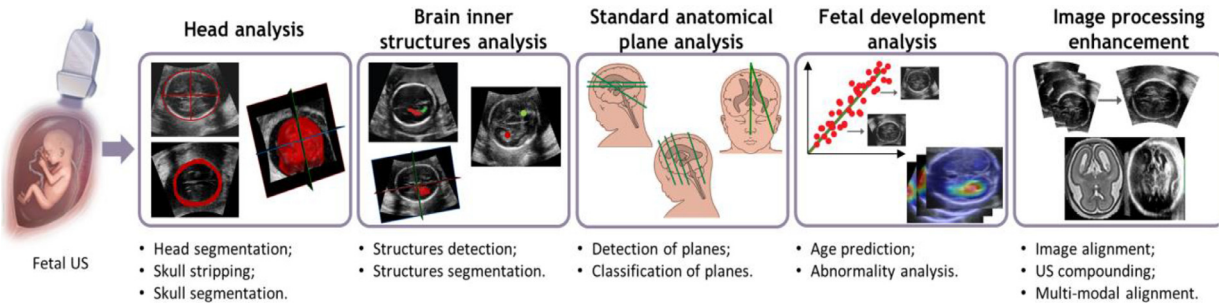

Fig. 1. Division by practical applications of image-based analysis of fetal head in US images.

meaningful information from it, allowing to improve the diagnosis and the patient's monitoring and facilitate the decision-making process in cases where treatment or intervention is required. However, naked-eye evaluation of US images is very challenging, being also time-consuming, labor-intensive, and highly prone to intra- and interobserver variability. For these reasons, robust semi- or automatic methods to process the image can aid fetal evaluation.

This work intends to summarize the state-of-the-art of image-based techniques to evaluate fetal head/brain in US. Despite few reviews were already developed for fetal brain MR imaging [9,10], and for fetal MR/US body [11], no review specifically focused on fetal head and brain analysis in US was previously performed. Thus, to the best of the knowledge, this is the first review addressing a complete analysis of the fetal head and brain in US. The methods reviewed were divided according to their practical clinical applications (Fig. 1), namely head analysis, brain inner structures analysis, standard anatomical plane evaluation, fetal development analysis, and image processing enhancement. Moreover, the reviewed methods are also categorized based on their main theoretical approach, according to the five main categories as suggested in [12]: Global intensity-based (G. Intensity-based), deformable models, learning-based, registration, and active shape models (ASM). Thus, the major contributions of this review are:

- A complete overview of the state-of-the-art methods on head/brain analysis in US images;
- An exhaustive analysis of each method based on its clinical application (Fig. 1) and theoretical approach;
- A comparison between the different approaches along with a discussion on the most appropriate methods for each application and future research topics.

The rest of the manuscript is organized as follows. In Section 2, a brief introduction to fetal US imaging for head/brain analysis is provided. In Section 3, the methodology used to conduct the present review is presented. In the following five sections, the clinical applications are individually addressed, namely fetal head analysis (Section 4), brain inner structure analysis (Section 5), standard anatomical plane analysis (Section 6), fetal head development analysis (Section 7), and image processing enhancement (Section 8). For each, the description of the reviewed methods, their technical and clinical validation, and discussion of their performance are addressed. Following, Section 9 focuses on the general discussion of the current state of research and future perspectives. Finally, the main conclusions are given in section 10.

2. Fetal imaging of head and brain

2.1. Anatomical structures and anatomical views

One of the structures evaluated in prenatal ultrasound is the fetal skull, where its shape and size are assessed usually using biometric measurements such as head circumference (HC), biparietal diameter (BPD), and occipitofrontal diameter (OFD) [13]. Besides the fetal skull, the nervous system (mainly the brain) is also evaluated. The fetal brain undergoes significant changes in both size and shape during fetal development, which are quantified to analyze brain development [14]. The brain structures sought in fetal US are lateral ventricles (LV), cavum septi pellucidi (CSP), thalamus (Th), cerebellum (Ce), choroid plexus (CP), and cisterna magna (CM), being their lengths/diameters usually estimated for brain evaluation [6]. A description of fetal brain structures can be found in Table 1.

When evaluated in 2D, the analysis of the structures is performed on the standard anatomical planes (see Fig. 2) [15,16]. From the axial view, three planes are usually assessed, namely the transventricular (TV), transthalamic (TT), and transcerebellar (TC) planes (Fig. 3). The TV plane is usually used for the visualization and measurement of the LV. Plus, it is also used to assess the CSP and CP. In the TT plane, structures such as the frontal horns of the LV, CSP, Th, and lateral sulcus (LS) can be analyzed. Moreover, HC, BPD, and OFD are estimated at this plane. The assessment of the TC plane includes the visualization of the frontal horns of the LV, CSP, Th, Ce, and CM. Thus, this plane is used to measure the diameter of the CM and the width of the Ce. From the coronal view, four different planes are usually evaluated, namely the transfrontal, transcaudate, coronal TT, and coronal TC planes. The transfrontal plane depicts structures such as the interhemispheric fissure, the frontal cortex, the frontal horns of the LV, and the ocular orbits while the transcaudate plane depicts the CSP, the anterior portion of the CC, and also the frontal horns of the LV. Using the coronal TT plane, the Th, the anterior portion of the CC, and CSP can be analyzed. The cerebellar hemispheres are evaluated in the TC plane. Finally, two sagittal planes are usually studied, namely the midsagittal (MS) and the parasagittal planes (PS). The assessment of the CC is performed in the MS plane, where midline structures of the brain are evaluated to diagnose midline deformations. In the PS plane, the entire LV can be evaluated, along with the CP.

2.2. Abnormal US findings

Several conditions are diagnosed by evaluating the fetal skull [17]. One severe condition evaluated is anencephaly, which is recognized by failure of development of the skull and consists in an absence of parts of the brain and skull. During US examination, this condition is diagnosed by evaluating if the bones of the cranium are deficient above the level of the orbits. Another condition is encephalocele, characterized by a defect of the skull resulting from nervous tissue that protrudes through skull openings, being visible on the US. Bone integrity and density can also be evaluated to find defects at the skull [3,18]. By analyzing fetal skull shape, cranial indexes can be estimated and cranial deformities such as scaphocephaly, brachycephaly, or plagiocephaly can be diagnosed [3,19]. Here, an elongated skull vault corresponds to scaphocephaly, a flattened skull indicates brachycephaly, and an asymmetric skull corresponds to plagiocephaly. Moreover, a lemon-

Table 1
Overview of Brain anatomical structures evaluated in fetal US.

Structure	Anatomical description	Ultrasound appearance	Abnormal US findings examples
Skull	Bone structure that protects the brain	Continuous highly hyperechogenic structure	Anencephaly, encephalocele, microcephaly, macrocephaly, plagiocephaly, scaphocephaly, brachycephaly
Lateral ventricles, LV	Structures filled with cerebrospinal fluid	Highly hyperechogenic at horns	Ventriculomegaly, hydrocephalus
Cavum septi pellucidi, CSP	Fluid filled cavity that separates both LV	Anechoic triangular-shaped under CC	Absence of CSP, holoprosencephaly, agenesis of CC
Thalamus, Th	Two oval structures of gray matter	Hypoechogenic structure	Holoprosencephaly
Cerebellum, Ce	Butterfly-shaped structure formed by hemispheres	Hemispheres connected by a hyperechogenic structure	Cerebellar hypoplasia, spina bifida, Arnold Chiari II and Dandy-Walker malformations
Choroid Plexus, CP	Located in the LV containing cerebrospinal fluid	Hyperechogenic structure within the LV	CP lesions
Cisterna Magna, CM	Fluid filled space posterior to the cerebellum	Anechoic structure	Spina bifida, Arnold Chiari II malformation
Corpus Callosum, CC	Fibrous structure connecting right and left brain	Hypoechogenic structure	Agenesis of CC

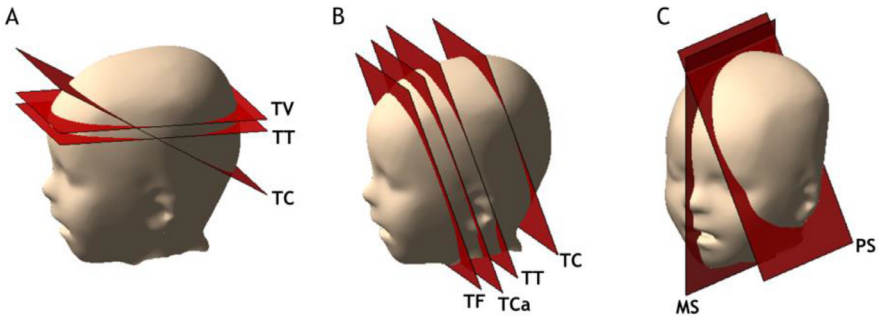

Fig. 2. Standard anatomical views for fetal head analysis. (A) Axial views; (B) Coronal views; (C) Sagittal views; TV – transventricular plane, TT – Transthalamic plane, TC – Transcerebellar plane, TCa – Transcaudate plane, TF – Transfrontal plane, MS – Midsagittal plane, PS – Parasagittal plane.

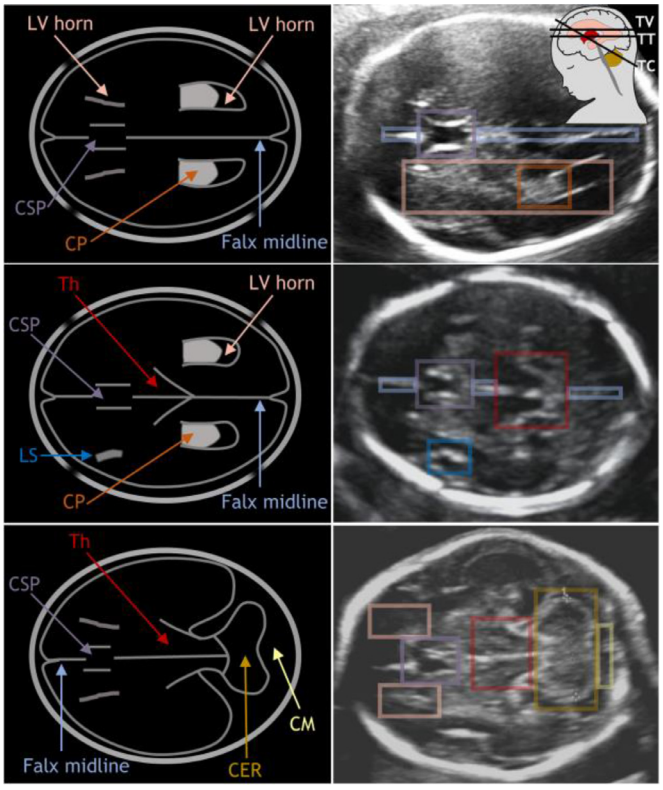

Fig. 3. Standard axial anatomical views. The first, second, and third row concern the TV, TT, and TC plane, respectively. The first column presents a scheme of the available features on each plane, while the second column is the real US image.

shaped head due to frontal bone scalloping can be also evaluated by ultrasound, indicating spinal dyspraphism and the Arnold Chiari II malformation. From skull size, conditions such as microcephaly or macrocephaly are evaluated by analyzing if the HC is below or above reference values, respectively [13].

Concerning the fetal CNS, brain abnormalities comprise a wide spectrum of conditions [14,17,20]. One of the most common problems detected is ventriculomegaly, which is an abnormally dilated LV [18]. When in the TV plane, this condition is diagnosed by measuring the ventricular atrium on an axis perpendicular to the long axis of the LV. In severe cases, ventriculomegaly can represent obstruction of the flow of cerebrospinal fluid and consequent raise of the pressure within the ventricular system, indicating a hydrocephalus condition.

Midline abnormalities are also detected by US, including holoprosencephaly which is a cephalic disorder that results from a failure of development of the normal forebrain. In US, this condition can be detected by the presence of a fused Th, absence of CSP, and a single dilated midline ventricle replacing the LV [20]. Agenesis or abnormal CC can also be found during the examination, consisting in the absence of the brain area that connects the two cerebral hemispheres [18]. During US examination, this condition can be perceived by the lack of visualization of CC in the midsagittal and coronal planes. The sonographic evaluation of the CM can also be used to detect abnormalities in the midline, such as enlarged CM or obliterated CM, which can indicate Arnold Chiari II malformation when accompanied with distortion of the cerebellum. Moreover, cerebellar hypoplasia can be associated with a Dandy-Walker malformation which affects brain development. Usually, cerebellar hypoplasia is diagnosed by measuring the transcerebellar diameter. Another condition is spina bifida, where an abnormal lemon-shaped head, an abnormal shaped CER, and an obliterated CM are found.

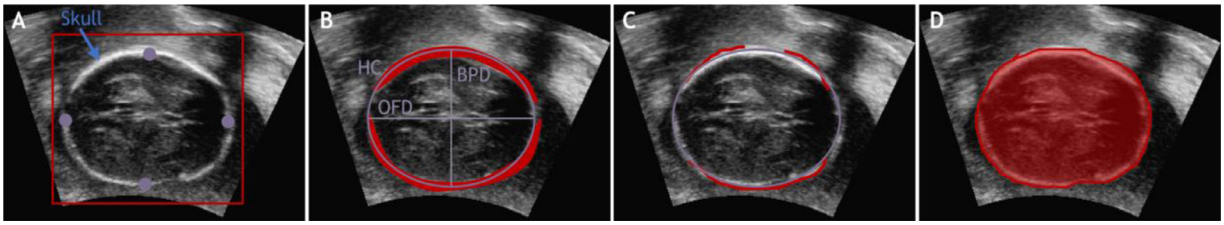

Fig. 4. Approaches for fetal head analysis. (A) Head location with a bounding box of the head ROI in red and landmarks at skull extremities in purple; (B) Skull segmentation with the segmentation result in red and an ellipse fitted to the segmentation in purple. HC corresponds to the perimeter of the ellipse and BPD and OFD corresponds to its minor and major axis, respectively; (C) Edge-based approach with the skull edges in red and an ellipse fitted to the edges; (D) Contour-based approach.

Finally, destructive lesions are also sought during fetal US examination, including tumors, cysts, or intracranial hemorrhage [18]. As a final remark, besides the use of 2D/3D US for detection of fetal abnormalities, Doppler US can also be used to detect vascular abnormalities, such as aneurysms, or anemia.

3. Review methodology

In this section, the methodology used for conducting the present review is described. A computer-assisted search was performed by the first author in the Scopus, Web of Science, and PUBMED databases using combinations of the following keywords: “fetal head”, “fetal brain”, “fetal standard anatomical planes”, “fetal neurodevelopment”, “ultrasound”, “segmentation”, and “classification”. The search was carried out to cover the period between 2010 and 2020. The articles were analyzed based on their title and abstract, allowing to select eligible articles. Excluded works included non-English language papers, patents, and papers that were not referent to the image processing topic. Moreover, US not related articles were excluded. Articles that presented scientific work in one of the five clinical applications using US were selected. Moreover, the reference list of relevant works was hand searched for additional literature. After removing duplicates, 126 papers were selected for full-text analysis. 109 of these 126 papers were reviewed and are described in this review.

4. Fetal head analysis

4.1. Overview of methods

Accurate head measurements are of high importance in obstetrics for fetal growth monitoring. Traditional clinical practice for head analysis includes the estimation of 2D measurements such as HC, BPD, and OFD from an ellipse representative of the fetal skull, manually fitted in the US image by sonographers. However, this process tends to be subjective and requires expertise. Moreover, when in 3D, manual shape analysis to quantify cranial deformities requires manual delineation of head contours, which is a difficult and time-consuming task. Thus, automatic methods for fetal head analysis have been proposed. Detection methods are the ones used to locate the head region or landmarks in the skull. Skull segmentation methods distinguish the skull bone structure from the rest of the image, normally followed by ellipse fitting approaches for biometry estimation. In its turn, edge-based methods only intend to perform a coarse detection of image features, e.g. partial skull edges, to be used for ellipse fitting. Finally, contour-based methods seek to find a closed outer contour of the skull with its fine details. An illustration of the types of head analysis approaches can be seen in Fig. 4.

An overview of the reviewed methods for head analysis is presented in Table 2, where the main category of the methods along with their description are presented. Note that some of the methods can be considered hybrids once the theoretical approach of the strategy involves methods and principles of more than one category. However, in the present state-of-the-art, the methods are included in the category that best fits their main theoretical approach. The required user interaction (UI) is also presented, being used the abbreviation A for fully automatic methods, MI when a manual initialization of the method is required (e.g. initial contour or seed point), and MR for works that manually define an ROI before applying the method.

4.1.1. Head detection methods

Khan et al. [21] and Sahli et al. [22] proposed to exploit simple image information to detect skull extremities. In [21], the Canny detector is used after morphological operations to detect the upper and lower skull boundaries. From each boundary, the midpoint is used as endpoints for BPD estimation. In [22], two additional landmarks for OFD endpoints are estimated, where hysteresis thresholding and log Gabor feature extraction are applied to detect the four landmarks. A head ROI is detected in the work of Baumgartner et al. [23], using a deep-learning (DL) approach. In this work, saliency maps are obtained from the most active feature neurons after processing a US image using a Convolutional Neural Network (CNN) applied for image classification. By thresholding the map, the ROI is obtained. In [24], a different network architecture was applied by the same team.

4.1.2. Skull segmentation methods

Considering the relevance of HC, BPD, and OFD measurements, several authors explored a rough skull segmentation approach followed by ellipse fitting. Satwika et al. proposed to use a simple thresholding approach to obtain a binary image of the skull, later applying an ellipse approximation method [25], Hough Transform (HT) [26], or randomized HT with particle swarm optimization techniques [27] to extract the final result. Threshold followed by HT was also applied by Sahli et al. [28,29]. While in [28] the HT is used to find a circular shape, in [29] an ellipse shape is found. Mathematical morphology was used by Liu et al. [30] to process the image and to obtain its maximum connected region (i.e. the skull). Constraining points in this region are used to improve the accuracy of the randomized HT approach. In [31], mathematical morphology was also applied by Marhaban et al. to segment the fetal skull, where direct least-square fitting on a skeletonized segmentation is used to find the ellipse, similarly to the work of Saii and Kraitem [32]. Ponomarev et al. [33] used shape descriptors to eliminate objects in an initial thresholded image. More recently, a different global intensity-based approach was proposed by Sree and Vasanthanayaki [34]. Here, a fuzzy connectedness segmentation approach is used, after definition of seed points by the user.

The major drawback of the abovementioned methods, especially the automatic ones, is the low robustness of pure global intensity-based approaches to noisy regions, leading to an over segmented skull and resulting in incorrect ellipsoid fitting. Thus, some works proposed to minimize this problem by restricting the image information before application of the global intensity-based method,

Table 2
Overview of fetal head analysis methods.

	Reference	Dim.	Category	Method initialization	Method final stage	UI
Det.	Khan et al. [21]	2D	G. Intensity-based	Threshold and morphology	Canny detector	A
	Sahli et al. [22]	2D	G. Intensity-based	Hysteresis threshold	Log Gabor feature extraction	A
	Baumgartner et al. [23, 24]	2D	Learning-based	–	CNN	A
Skull segmentation-based	Satwika et al. [25–27]	2D	G. Intensity-based	Threshold	Ellipse fitting/HT	A
	Sahli et al. [28, 29]	2D	G. Intensity-based	Threshold	HT	A
	Liu et al. [30]	2D	G. Intensity-based	Morphology	Constrained Randomized HT	A
	Marhaban et al. [31]	2D	G. Intensity-based	Morphology	Least Square Fitting	A
	Saii and Kraitem [32]	2D	G. Intensity-based	Threshold and morphology	Least Square Fitting	A
	Ponomarev et al. [33]	2D	G. Intensity-based	Threshold and shape descriptors	Contrast-based pixel score	A
	Sree and Vasanthanayaki [34]	2D	G. Intensity-based	Fuzzy connectedness segmentation	Least Square Fitting	MI
	Ma'Sum et al. [35]	2D	G. Intensity-based	Adaboost classifier and threshold	Randomized HT	A
	Jatmiko et al. [36]	2D	G. Intensity-based	Adaboost classifier and threshold	Randomized HT	A
	Imaduddin et al. [37]	2D	Learning-based	Adaboost classifier	Randomized HT	MR
	Anto et al. [38]	2D	Learning-based	Feature extraction	RF	A
	Namburete and Noble [39]	2D	Learning-based	Simple linear iterative clustering	RF	A
	Rahmatullah et al. [40]	2D	Learning-based	Simple linear iterative clustering	RF	A
	Cerrolaza et al. [41, 47]	3D	Learning-based	Structured feature extraction for RF	RF/CNN	A
	Perez-Gonzalez et al. [42, 43]	3D	Learning-based	Feature extraction	SVM/RF	A
	Heuvel et al. [44]	2D	Learning-based	CNN and U-Net	Least Square Fitting	A
	Kim et al. [46]	2D	Learning-based	Image transformation and U-Net	Least Square Fitting	MI
Edge-based	Rahayu et al. [48]	2D	G. Intensity-based	Morphology and canny detector	Integral projection	A
	Banerjee and Krishnan [49]	2D	G. Intensity-based	Generation of diffusion images	Diffusion and RANSAC	A
	Ni et al. [50]	2D	G. Intensity-based	Adaboost classifier and phase analysis	Iterative Randomized HT	A
	Li J et al. [51]	2D	G. Intensity-based	RF and phase-based analysis	Fast ellipse fitting	A
	Yaqub et al. [52]	2D	G. Intensity-based	Phase analysis	Template correlation	A
	Foi et al. [53, 54]	2D	G. Intensity-based	Random ellipse fitting	Gaussian elliptical path	A
	Kusuma et al. [55]	2D	G. Intensity-based	Random ellipse fitting	Gaussian elliptical path	A
	Ma'Sum et al. [56]	2D	G. Intensity-based	Random ellipse fitting	Gaussian elliptical path	A
	Stebbing and McManigle [57]	2D	Learning-based	Phase-based model and RF	Dual ellipse fitting	A
	Zhang et al. [58]	2D	Learning-based	Texton-based edge detection and SVM	Least Square Fitting	A
	Heuvel et al. [59]	2D	Learning-based	RF	HT and dynamic programming	A
Contour-based	Ciurte et al. [60, 61]	2D	G. Intensity-based	Ellipses in head and background	Min-cut algorithm	MI
	Sun [62]	2D	G. Intensity-based	Circular shortest path	Gradient-based edge detection	A
	Chen et al. [63]	3D	Def. models	Eye location and template registration	Active contours	A
	Perez-Gonzalez et al. [64]	2D	Def. models	Texture and morphological analysis	Active contours	A
	Rawat et al. [65]	2D	Def. models	Threshold	GVF	A
	Rong et al. [66]	2D	Def. models	Initial contour	Learning-based GVF	MI
	Gadagkar and Shreedhara [67]	2D	Def. models	Initial contour	Level-set	MI
	Rajinikanth et al. [68]	2D	Def. models	Jaya algorithm and Otsu threshold	Level-set	A
	Namburete et al. [69]	3D	Def. models	Surface initialization	Template deformation	MI
	Cuingnet et al. [70]	3D	Def. models	Ellipsoidal shell model	Template deformation	A
	Wu et al. [71]	2D	Learning-based	–	Cascade FCN	A
	Sinclair et al. [72]	2D	Learning-based	–	FCN	A
	Yaqub et al. [73]	2D	Learning-based	–	CNN	A
	Xie et al. [74]	2D	Learning-based	–	CNN	A
	Al-Bander et al. [75]	2D	Learning-based	–	Mask R-CNN	A
	Sobhaninia et al. [77, 78]	2D	Learning-based	–	Multi-task LinkNet/ LinkNet	A
	Huang et al. [79]	3D	Learning-based	–	U-Net	A
	Ye et al. [80]	2D	Learning-based	–	U-Net	A
	Budd et al. [81]	2D	Learning-based	–	Probabilistic U-Net	A
	Moser et al. [82]	3D	Learning-based	–	U-Net	A
	Yang et al. [83]	3D	Learning-based	–	Attention encoder-decoder	A
	Liu et al. [84]	2D	Learning-based	–	SAFNet	A

A: Automatic method, MI: semiautomatic method (manual initialization), MR: semiautomatic method (ROI definition).

by firstly finding an ROI of the head (see Fig. 5). Ma'Sum et al. [35] and Jatmiko et al. [36] exploited the Adaboost classifier with Haar features to obtain the head's ROI. In [37], Imaduddin et al. proposed to use the same classifier to binarize the skull. In [38], Anto et al. used a Random Forest (RF) classifier to segment the skull using image intensity as feature. A combination of unsupervised and supervised learning was proposed by Namburete and Noble [39]. Here, a simple linear iterative clustering method is used to create pixel clusters. Afterward, local statistics and shape information are used in an RF classifier, along with unary, binary, and Haar features, to obtain the final skull segmentation. A similar approach was proposed by Rahmatullah et al. [40], where image moment features were added to the RF approach. In [41], Cerrolaza et al. proposed a variant of the traditional RF (termed structured geodesic RF) that integrated semantic and structural information to segment the skull in 3D US volumes. 3D skull segmentation was also addressed by Perez-Gonzalez et al., where features related to texture, intensity, and edges are used in a Support Vector Machine (SVM) classifier [42] and RF classifier [43].

Despite the higher accuracy of learning methods compared with global intensity-based methods, they are highly dependent on the feature extraction stage. Thus, Deep Learning (DL) approaches were proposed. In [44], Heuvel et al. used CNN to classify the US image concerning the presence or not of the fetal head. For the images where the head was detected, a network inspired in the U-Net [45] was used to segment the skull. U-Net was also used by Kim et al. [46]. However, here a preprocessing step is applied to differentiate tissue patterns according to US wave propagation. US physics was also used by Cerrolaza et al. [47] to solve the problem of partial skull segmentation verified in the remaining methods. Here, a two-stage CNN is used, partially segmenting the skull in the first stage, and then angle incidence and shadow casting infor-

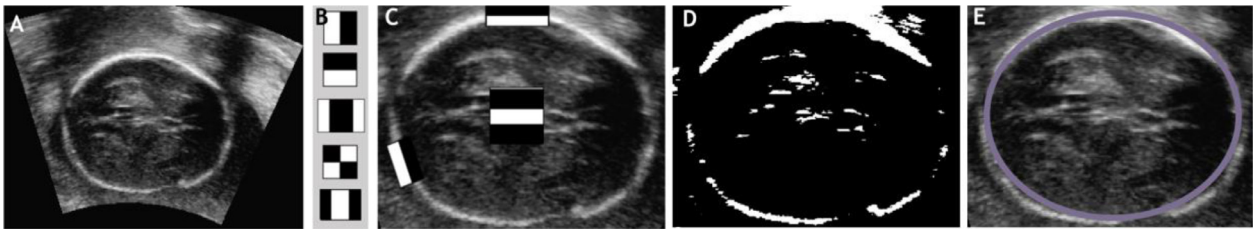

Fig. 5. Illustration of one example of head analysis method that uses a classification approach to detect the head and a global intensity-based method to segment the head. (A) Original US image; (B) Haar features used by several classification methods for fetal head segmentation/detection; (C) Head ROI after application of a classification approach using the Haar features (e.g. Adaboost classifier); (D) Binary image after thresholding (C); (E) Ellipse fitted the skull resulting from searching an ellipse shape in (D) (e.g. HT).

mation are added to the second stage to obtain the final segmentation.

4.1.3. Edge-based methods for head analysis

Instead of using skull segmentation to perform ellipse fitting, some methods explored different image features, e.g. skull edges. Rahayu et al. [48] used the Canny detector to find the edges of the skull in a morphological processed image, using an integral projection method to find points to fit the ellipse. A different approach was proposed by Banerjee and Krishnan [49] where multi-level diffusion images were created and the RANSAC technique was applied to obtain a consensus of the generated maps to perform the final ellipse fitting. Instead of finding edges using intensity information, several works proposed to use phase-based filters. Indeed, phase-based methods showed high accuracy and good response to speckle noise in US images, being useful to improve edge detection. Thus, Ni et al. [50] and Li J et al. [51] proposed to use this type of method to detect skull edges. Both methods performed detection of head's ROI before applying edge detection, using Adaboost classifier [50] and RF [51]. A phase-based image was also used by Yaqub et al. [52]. However, a template-based approach was proposed, where normalized cross-correlation between a set of skull templates and the phase-based image was evaluated to find the best template. Foi et al. [53] proposed a new way to represent the skull, using Difference-of-Gaussians (DoG) filter, considering that the skull can be represented as a gaussian-like curve with higher intensities than its surrounding tissues. An optimization procedure is applied to a random initialization of the DoG model to obtain the final ellipse. A more efficient optimization was proposed by the same authors in [54], while Kusuma et al. [55] explored nature-based optimizations and Ma'Sum et al. [56] investigated particle swarm optimization.

Machine learning methods were also used to compute the edge map. Stebbing and McManigle [57] investigated RF classifiers, where a boundary fragment model is constructed using phase-based image analysis and then incorporated into the RF to detect skull edges for ellipse fitting. In [58], Zhang et al. detected skull edges using texton features integrated into an SVM framework. In [59], RF was used by Heuvel et al. to compute the likelihood of a pixel belonging to the skull. Afterward, skull edges are searched using dynamic programming.

4.1.4. Contour-based methods for head analysis

Ciurte et al. [60] proposed to use an approach called patch-based continuous MinCut for skull's contour extraction. In this method, two ellipses corresponding to the fetal head and background are drawn in the image, and a continuous MinCut partition is used to obtain the skull contour through energy minimization. In [61], a new minimization algorithm that speeds up the optimization process was proposed. A graph-based method was also proposed by Sun [62], where the circular shortest paths method was used to iteratively find the skull's boundaries, which corresponds to the brightest optimal path. For refinement, an ellipse is fitted to the method's result and the outer skull edge is retrieved by computing the image gradient in the radial direction.

Deformable models were also applied for skull boundary extraction. This type of methods overcome the lack of robustness to noise of global intensity-based approaches, while obtaining a smooth and gapless segmentation. One illustration of a deformable model approach to segment the fetal head is presented in Fig. 6. Active contours were used by Chen et al. [63]. Here, an initial method based on Gabor-features was applied to detect the eyes' position, later using it to detect the head pose. Once detected the pose, a feature-based registration with a model is used as the initial surface for the active contour, being the contour evolved towards the skull boundary using intensity and edge features. In the work of Perez-Gonzalez et al. [64], texture maps were retrieved from the original image and combined in one map processed using threshold and morphology. An ellipse is detected in the map and used as an initial contour for an active contour. Other works proposed Gradient Vector Flow (GVF) to drive the active contour. In Rawat et al. [65], binarization is firstly applied to the image, and the final segmentation is obtained using a GVF computed from the image edge map. GVF was also studied by Rong et al. [66], were the gradient maps are inferred using a CNN. Instead of active contours, Gadagkar and Shreedhara [67] explored the topological flexibility of level-sets with reaction-diffusion optimization process. Rajinikanth et al. [68] also researched level-sets to obtain the skull contour, firstly applying a combination of the Chan-Vese and Jaya-algorithm to generate a binary image with an initial contour of the fetal head. The last type of deformable models proposed in the literature for fetal head extraction was template deformation. Namburete et al. [69] deformed a manually fitted surface towards the skull boundary using phase-based image features. In [70], Cuingnet et al. proposed to apply global and local non-rigid deformations to a previously generated template for 3D skull segmentation. The initial template was obtained by detecting an ellipsoidal model in the image based on the response of a plate detector, avoiding the need for manual surface fitting.

More recently, DL has been applied to segment the fetal head, usually in a skull stripping approach. In [71], Wu et al. proposed a cascaded Fully Convolutional Network (FCN) to obtain a dense prediction map of the fetal head. Plus, an auto-context scheme was used to obtain refinement of the map across different stages. An FCN architecture was also studied by Sinclair et al. [72] to obtain a binary image with the fetal head, while Yaqub et al. [73] and Xie et al. [74] explored a CNN architecture. In [75], a CNN is firstly applied by Al-Bander et al. for feature extraction, being used as a backbone for a faster regional CNN (R-CNN) that detects the head's ROI. After head detection, a mask R-CNN is used to obtain the final segmentation. An architecture based on the LinkNet [76] was used by Sobhaninia et al. [77]. Here, a multi-task DL was implemented to simultaneously predict a mask of the skull and to tune the parameters of an ellipse fitted to the obtained mask, considering that

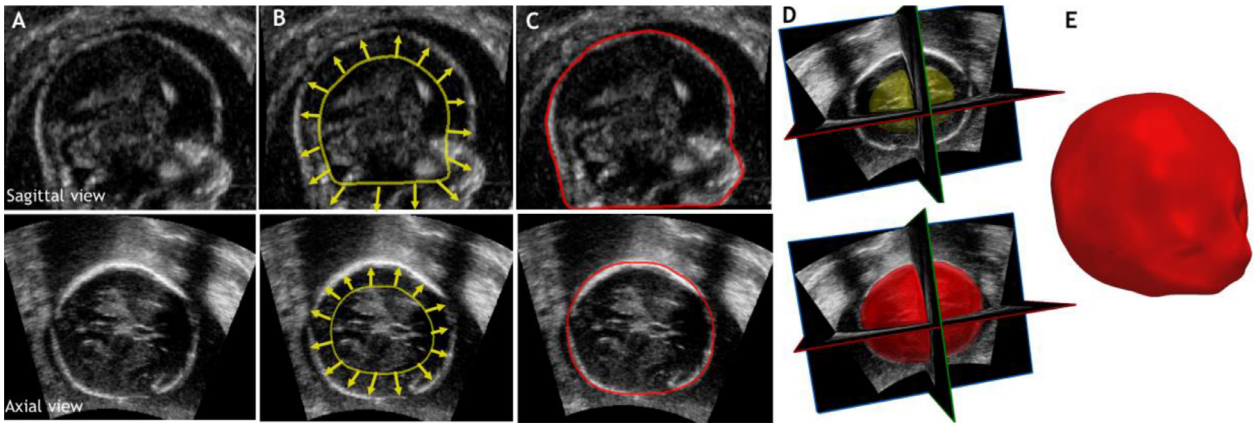

Fig. 6. Illustration of an active contour approach to segment the fetal head in 3D images. (A) Sagittal and axial views of the volume; (B) Initial contour (yellow) for the segmentation process. The yellow arrows represent the forces that drive the contour to evolve towards the skull; (C) Final contour (red) resulted from the segmentation process; (D) 3D representation of the initial and final contours; (E) Final 3D model of the fetal head.

a multi-task formulation can lead to better results when compared with a single task. In [78], a lighter network to perform the head segmentation task was proposed by Sobhaninia et al. The U-Net architecture was used by Huang et al. [79], Ye et al. [80], Budd et al. [81], and Moser et al. [82]. In [80], dilated convolutions were proposed to obtain a larger receptive field of the network. In [81], a probabilistic U-Net was applied, where different plausible segmentations are obtained and used to estimate HC. In [82], the brain mask is extracted. Yang et al. [83] explored a cascade of encoder-decoder deep architectures, where a hybrid attention scheme was integrated into the network to select discriminative features and enhance the feature maps in key sites. The addition of attention modules in a network was also proposed by Liu et al. [84], where a scale attention feature pyramid network called SAFNet was used for head segmentation.

4.2. Performance assessment

In Table 3, the performance assessment of the methods for head analysis reviewed in Section 4.1 is presented. Here, performance assessment was divided into region-based, contour-based, and biometry analysis. While region-based analysis includes metrics that indicate the overlap between the segmentation result and the ground-truth, contour-based metrics assess the distances between their contours. Biometry analysis evaluates the errors between HC, BPD, and OFD estimated automatically and the manual ones.

To limit the scope of the comparison between methods, a few papers were not included in the table. Publications that did not mention the number of images evaluated or that only performed qualitative evaluation are not shown. Plus, publications that do not present direct evaluation metrics for all images evaluated (i.e. its average value) were excluded. If the evaluation was performed against several ground-truths, only one is present. Similarly, if several experiments were conducted, only the best is shown. One important aspect that should be noted during the analysis of the performance assessment table is that accuracy assessment varies between the reviewed papers, which results in a lack of standardized evaluation in terms of metrics and hampers the direct comparison between methods.

4.3. Discussion

After analyzing the reviewed methods for head analysis (Table 2 and Table 3), it is possible to verify that simple global intensity-based methods are often used, namely for the ones that seek to segment the skull or to find its edges. Image-driven techniques present as advantages their simple theoretical approach, while being accurate to segment homogeneous objects. Indeed, the skull appears as a highly bright object within the image and the contrast between the fetal head and the surrounding amniotic fluid is often high, allowing the use of simple intensity-based methods. Moreover, the fetal skull present identifiable features that can be retrieved from the image (i.e. its high intensity). Learning-based approaches that use these handcrafted features were also used to classify the skull in the US images, often achieving higher level of accuracy in comparison with simple intensity-based methods. Moreover, the trend was to improve the robustness of the machine learning techniques during the reviewed period, adding other features that such as geometry or texture. However, skull occlusions are frequently found in these images, varying their appearance across different fetal poses and gestational ages. These missing boundaries hampers the segmentation of the entire fetal skull as a unique structure. To allow the extraction of biometric measurements and correct evaluation of the fetal head from these partial segmentations, shape information is integrated into this type of methods, by searching for an ellipsoid shape in the partial map. In fact, this process mimics the traditional manual clinical practice. Within the methods used to integrated shape prior information, HT or other variants of this method are usually applied [25-30,50,59]. Another challenge in fetal skull segmentation in US is that image artifacts or other anatomical structures can present similar intensities to the skull. In such cases, simple global intensity-based and traditional learning-based methods are likely to fail since they cannot distinguish the artifacts from the fetal structure, generating noisy segmentation maps and hampering ellipsoid fitting. To solve this issue, some methods applied a pre-processing stage where the ROI of the fetal head is found, having the advantage of limiting the image area to be processed [37,50,51]. However, simple global intensity-based and traditional learning-based methods are still applied after this pre-processing stage, not allowing to retrieve the fine details of the skull shape due to the missing boundaries, which can be important to analyze its specific details. Thus, contour-based methods that have the goal of segmenting the head as an entire structure with its real contours were also proposed in the literature. Within these methods, deformable models have been widely explored, taking as advantage their robustness to noise and lower sensitivity to weak boundaries. However, their sensitivity to the initial contour and to local minimums remains a drawback for segmentation tasks. On other hand, machine learning, specifically DL, was also applied to create a model of the entire head shape. Considering the improvement of computing capa-

Table 3
Performance assessment of head analysis methods.

Reference	N	GA (weeks)	Region evaluation		Contour evaluation		Biometry evaluation	
			Metric	Value	Metric	Value	Metric	Value
Khan et al. [21]	27	18–34	–	–	–	–	ME_{BPD}	0.72 ± 3.62 mm
Baumgartner et al. [24]	510	18–22	IOU_{ROI}	0.73 ± 0.11	–	–	–	–
Satwika et al. [26]	60	2nd,3rd	–	–	–	–	ME_{BPD}	2.19 mm
							ME_{HC}	20.41 mm
Satwika et al. [27]	72	2nd,3rd	–		–	–	ME_{BPD}	3.87 mm
							ME_{HC}	14.6 mm
Sahli et al. [29]	266	19	AC_{head}	96.6 ± 0.5%	–	–	–	–
			RE_{head}	96.1 ± 0.4%				
			SP_{head}	98.1 ± 0.7%				
			DSC_{head}	98.7 ± 0.4%				
Ponomarev et al. [33]	90*#	21–33	PR_{head}	87.29 ± 12.79%	ASD	2.83 ± 3.83 mm	–	–
			RE_{head}	88.06 ± 12.88%	HD	6.87 ± 9.82 mm		
			SP_{head}	99.48 ± 1.11%	RMSD	3.55 ± 5.21 mm		
			DSC_{head}	92.53 ± 10.22%				
Sree and Vasanthanayaki [34]	50	–	PR_{head}	96%	HD	2.16 mm	–	–
			RE_{head}	98%	RMSD	1.08 mm		
			SP_{head}	98%				
Jatmiko et al. [36]	100	2nd,3rd	–	–	–	–	ME_{BPD}	2.20 mm
							ME_{HC}	82.14 mm
Nadiyah et al. [140]	10	–	–	–	–	–	AC_{HC}	> 92.86%
Anto et al. [38]	50	–	DSC_{skull}	75%	–	–	–	–
Namburete and Noble [39]	10*	25–34	AC_{skull}	97.22%	–	–	–	–
			PR_{skull}	99.01%				
			RE_{skull}	98.11%				
Rahmatullah et al. [40]	100	–	AC_{skull}	96.92%	–	–	–	–
			RE_{skull}	41.34%				
			SP_{skull}	99.55%				
			$F1_{skull}$	53.51%				
Cerrolaza et al. [41]	10	20–30	DSC_{skull}	80 ± 3%	–	–	–	–
			JI_{skull}	65 ± 4%				
			RE_{skull}	80 ± 7%				
			SP_{skull}	99 ± 1%				
			AC_{skull}	98 ± 1%				
Cerrolaza et al. [47]	14	20–36	DSC_{skull}	83 ± 6%	ASD	0.98 ± 0.52 mm	–	–
			JI_{skull}	70 ± 8%				
Perez-Gonzalez et al. [43]	5	20–24	DSC_{skull}	86.8 ± 3.5%	HD	5.9 ± 1 mm	–	–
			AUC_{skull}	83.7 ± 3.4%				
Heuvel et al. [44]	36	20–40	–	–	–	–	ME_{HC}	−3.0 ± 13.3 mm
							MAE_{HC}	10.3 mm
Kim et al. [46]	70	2nd,3rd	DSC_{head}	95.39 ± 0.02%	–	–	–	–
Ni et al. [50]	175	17–38	–	–	–	–	ME_{HC}	2.84 mm
							MAE_{HC}	5.58 mm
Li et al. [51]	145	18–33	PR_{head}	96.84 ± 2.99%	ASD	1.74 ± 1.35 mm	–	–
			RE_{head}	96.80 ± 2.83%	HD	1.78 ± 1.58 mm		
			SP_{head}	96.72 ± 3.12%	RMSD	1.77 ± 1.37 mm		
			DSC_{head}	96.66 ± 3.15%				
Foi et al. [53]	90*	21–33	PR_{head}	95.72 ± 1.92%	ASD	0.88 ± 0.53 mm	–	–
			RE_{head}	98.51 ± 1.20%	HD	2.16 ± 1.44 mm		
			SP_{head}	98.28 ± 1.26%	RMSD	1.08 ± 0.69 mm		
			DSC_{head}	97.80 ± 1.04%				
Foi et al. [54]	90*	21–33	DSC_{head}	97.73 ± 0.89%	ASD	0.91 ± 0.47 mm	ME_{BPD}	−1.02 ± 0.97 mm
					HD	2.26 ± 1.47 mm	ME_{OFD}	−0.87 ± 2.84 mm
							ME_{HC}	−2.34 ± 3.72 mm
Kusuma et al. [55]	86	2nd,3rd	DSC_{head}	86.42 ± 11.69%	–	–	ME_{BPD}	3.25 mm
							ME_{HC}	16.82 mm
Stebbing and McManigle [57]	90*	21–33	PR_{head}	94.63 ± 1.45%	ASD	1.07 ± 0.39 mm	–	–
			RE_{head}	98.86 ± 1.26%	HD	2.59 ± 1.14 mm		
			SP_{head}	97.53 ± 1.29%	RMSD	1.29 ± 0.51 mm		
			DSC_{head}	97.23 ± 0.77%				
Zhang et al. [58]	10	20–35	PR_{head}	94.91 ± 2.57%	ASD	0.87 ± 0.48 mm	ME_{BPD}	0.26 ± 2.46 mm
			RE_{head}	99.16 ± 1.18%	HD	2.37 ± 1.46 mm	ME_{OFD}	−0.65 ± 4.61 mm
			SP_{head}	99.19 ± 0.62%	RMSD	1.08 ± 0.64 mm	ME_{HC}	−0.22 ± 9.53 mm
			AC_{head}	99.19 ± 0.47%				
Heuvel et al. [59]	335	12–20	DSC_{head}	97.0 ± 2.8%	HD	2.0 ± 1.6 mm	ME_{HC}	0.6 ± 4.3 mm
							MAE_{HC}	2.8 ± 3.3 mm
Ciurte et al. [60]	90*	21–33	PR_{head}	89.53 ± 2.81%	ASD	2.10 ± 0.69 mm	–	–
			RE_{head}	90.19 ± 3.05%	HD	4.6 ± 1.64 mm		
			SP_{head}	99.62 ± 0.48%	RMSD	2.47 ± 0.83 mm		
			DSC_{head}	94.45 ± 1.57%				
Sun [62]	90*	21–33	PR_{head}	94.15 ± 2%	ASD	1.19 ± 0.54 mm	–	–
			RE_{head}	95.63 ± 2.46%	HD	3.02 ± 1.55 mm		
			SP_{head}	99.12 ± 1.12%	RMSD	1.48 ± 0.71 mm		
			DSC_{head}	96.97 ± 1.07%				

(*continued on next page*)

Table 3 (*continued*)

Reference	N	GA (weeks)	Region evaluation		Contour evaluation		Biometry evaluation	
			Metric	Value	Metric	Value	Metric	Value
Chen et al. [63]	220_{slices}	20–24	DSC_{head}	96.55 ± 0.7%	MAE	1.82 ± 0.32 pixel	–	–
Perez-Gonzalez et al. [64]	10_{Seg} 24_{Biom}	17–30	PR_{head} DSC_{head}	94.61 ± 1.72% 97.19 ± 0.97%	HD	2.64 ± 0.57 mm	ME_{BPD} ME_{HC}	−2.72 ± 2.03 mm −2.73 ± 2.04 mm
Rong et al. [66]	335+	12–20	DSC_{head}	95.49 ± 4.11%	HD	2.44 ± 1.96 mm	ME_{HC} MAE_{HC}	−1.05 ± 3.38 mm 2.45 ± 2.55 mm
Rajinikanth et al. [68]	25+	12–20	PR_{head} RE_{head} SP_{head} AC_{head} DSC_{head} JI_{head}	99.13% 86.89% 99.93% 99.93% 94.27% 89.16%	–	–	–	–
Wu et al. [71]	236	19–40	DSC_{head} JI_{head}	98.43% 96.90%	ASD	2.05 mm	–	–
Sinclair et al. [72]	539	18–22	DSC_{head}	98.1 ± 0.7%	–	–	ME_{BPD} MAE_{BPD} ME_{HC} MAE_{HC}	0.13 ± 0.91 mm 0.68 ± 0.62 mm 0.54 ± 2.28 mm 1.80 ± 1.49 mm
Yaqub et al. [73]	5000	–	PR_{head} RE_{head} DSC_{head} JI_{head}	95.1 ± 2.8% 98.9 ± 1.5% 96.9 ± 1.6% 94.0 ± 2.1%	–	–	–	–
Xie et al. [74]	1300	18–32	PR_{head} RE_{head} DSC_{head}	97.9% 90.9% 94.1%	–	–	–	–
Al-Bander et al. [75]	335+	12–20	DSC_{head}	97.73 ± 1.32%	ME MAE HD	1.49 ± 2.85 mm 2.33 ± 2.21 mm 1.39 ± 0.82 mm	–	–
Sobhaninia et al. [77]	2206	–	DSC_{head}	96.84 ± 2.89%	HD	1.72 ± 1.39 mm	ME_{HC} MAE_{HC}	1.13 ± 2.6 mm 2.12 ± 1.87 mm
Sobhaninia et al. [78]	1998	–	DSC_{head}	93.75%	HD	3.70 mm	ME_{HC} MAE_{HC}	1.53 mm 2.27 mm
Huang et al. [79]	45	20–29	IOU_{head}	86.5 ± 5.1%	PD	1.6 ± 1.0 mm	–	–
Ye et al. [80]	2000	–	PR_{head} RE_{head} DSC_{head} $F1_{head}$	97.9% 90.9% 94.3% 94.1%	–	–	–	–
Budd et al. [81]	540	18–22	DSC_{head}	98.2 ± 0.8%	HD	1.295 ± 0.66 mm	MAE_{HC}	1.808 ± 1.65 mm
Moser et al. [82]	300*	14–31	DSC_{brain} SC_{brain}	94 ± 2% 95 ± 2%	PD_{brain} HD	1.36 ± 0.72 mm 4.609 mm	–	–
Yang et al. [83]	50	20–31	DSC_{head} JI_{head}	96.05% 92.42%	ASD HD	0.4793 mm 4.609 mm	–	–

N: number of images; AC: accuracy, AUC: area under curve, DSC: Dice similarity coefficient, F1: F1-score, IOU: intersection over union, JI: Jaccard index, PR: precision, RE: recall, SP: specificity; ASD: average symmetric distance, HD: Hausdorff distance, PD: point/landmark distance, RMSD: root mean square distance; MAE: mean absolute error, ME: mean error. *INTERGROWTH-21st data, #*Challenge US: Biometric Measurements from Fetal Ultrasound Images* challenge, +*HC18* challenge.

bilities and rapid development in terms of network architectures or models, DL-based approaches have now superseded the image processing field. Thus, in the recent years, research has been focused on DL for fetal head segmentation, due to the capability of these strategies to obtain feature representations directly from the images without the need of handcrafted features, while achieving accurate and fast results [72-75, 77-84]. The first approaches to segment the fetal head using DL consisted of networks commonly used to perform image classification tasks followed by upsample layers to output an image with the same size as the input image. The main advantage of using this type of networks is that since their backbone is commonly used for other computer vision tasks, pre-trained weights for high-level feature extraction were used in such methods (mostly from ImageNet [85]), which can be an advantage if the size of the training dataset is reduced. However, the most recent DL-based approaches to segment the fetal head consisted in encoder-decoder architectures (e.g. U-Net [45]) to enable precise localization of the fetal head pixels. One interesting aspect that was retrieved from the reviewed papers is that only one approach found in the literature combined the task of head segmentation with the task of ellipse finding in the same network. Indeed, this multitask DL solution seems to be an interesting approach since training the ellipse parameters can aid in the task of head segmentation to output anatomical coherent results from where the biometric parameters can be estimated.

One important aspect that should be analyzed in the methods reviewed for fetal head segmentation is their final goal. Most of the methods reviewed in Section 4.1 were applied for biometry estimation (see Fig. 7). As already mentioned, biometric measurements of fetal head are crucial indicators for maternal and fetal health monitoring during pregnancy. However, only a few works focused on head segmentation in 3D, which can be critical to correctly evaluate its entire shape. In fact, despite 2D measurements could be used to infer some head shape conditions, such as cranial deformations, 3D models of the fetal head can allow the development of new analysis tools. However, from the reviewed methods, only a few can be directly used for the assessment of cranial deformations. Concerning the remaining head analysis methods, some were proposed with the final goal of estimating fetal development (i.e. GA estimation and abnormality classification), others seek to be used as a preprocessing step (i.e. skull stripping approach) for brain structures detection/segmentation and standard anatomical plane analysis, and others are used during image enhancement techniques (Fig. 7).

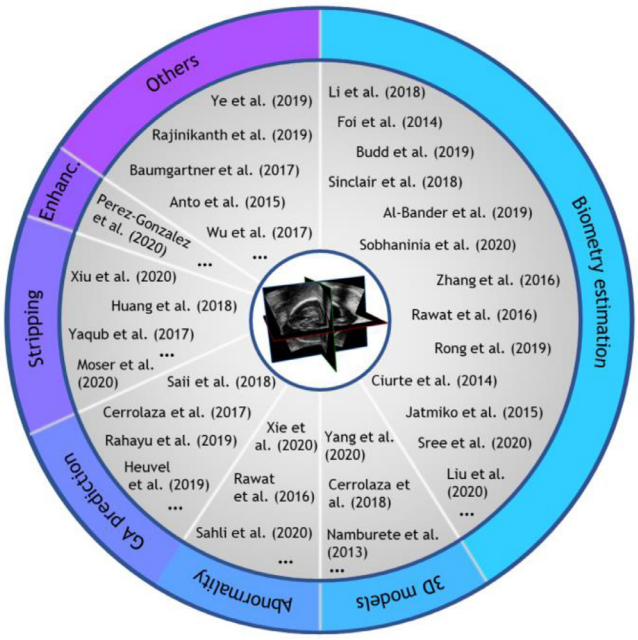

Fig. 7. Division of the reviewed methods for head analysis according to their goal. (Only few methods are showed in the figure for sake of exemplification).

5. Brain inner structures analysis

5.1. Overview of methods

Assessment of brain inner structures is essential to evaluate fetal condition and to find the best anatomical plane for qualitative and quantitative evaluation. State-of-the-art methods regarding this topic can be divided into two groups: (i) detection and (ii) segmentation. Detection methods are the ones used to detect the structure, with a bounding box or a landmark. Segmentation methods have the goal of obtaining anatomical models of the structures. An overview of literature methods is presented in Table 4.

5.1.1. Brain structures detection methods

Machine learning approaches have been widely proposed to detect brain structures in fetal US, either for landmark/centroid or ROI detection. For centroid detection, Yaqub et al. [86] proposed to use an RF that combines image features with the relative position of the structures to detect the center point of brain structures. Ce, CSP, and the posterior ventricle cavity (PVC) were addressed in this work. In [87], a patch-based iterative network was proposed by Li Y et al. to detect landmarks on the LV, Ce, and CSP, along with landmarks on the skull. In this work, the network guides an initial patch towards the landmark using a CNN that learns the spatial relation between an image patch and the landmark positions. Moreover, anatomical constraints among landmarks were also imposed to improve detection accuracy. Alansary et al. [88] proposed to use reinforcement learning based on deep Q-networks for landmark detection.

Other methods were applied for anatomical bounding box detection. Sofka et al. [89] estimated the position, orientation, and scaling of the bounding box of the structures using an integrated detection network based on discriminative classifiers. A hierarchical scheme is applied to firstly detect the Ce pose and then search for CC using Ce as prior. In [90], an extension of the previous method is proposed, where the location and size of Ce, CM, LV, CC, and CP are sequentially estimated. In [79], a DL approach termed a view-based projection network was proposed by Huang et al. to detect the bounding box of CSP, CE, CM, LV, and Th, after head segmentation. A 2D U-Net is used to scan the 3D volume on each view, estimating 3D positions from 2D predictions obtained on the three anatomical views. Known state-of-the-art object detection methods were applied by some authors for brain structures detection (see Fig. 8). In [91], Luo et al. proposed a Region Proposal Network (RPN) to locate the CSP, Th, CP, third ventricle, brain midline, and LS. After using a feature extraction network, a feature pyramid network is used to extract candidate anchors to the RPN. In [92], Lin et al. used the faster R-CNN, which combines R-CNN with RPN, to detect the same anatomical structures. A clinical prior knowledge module was added to improve the detection accuracy in [93]. The You Only Look Once (YOLO) algorithm was researched by Ramos et al. in [94] to detect CE bounding box.

5.1.2. Brain structures segmentation methods

A global intensity-based approach was proposed by Annangi et al. [95] to segment the third ventricle. After finding the skull based on the work in [49], phase congruency was applied to the original image to generate edges inside the skull, being the edges more symmetric to the skull ellipse assumed to be the ventricle. Liu et al. [30] segmented the Ce with an active contour method. Firstly, a constrained probabilistic boosting classifier was applied for Ce detection in multiple 2D slices, using information of the previously detected head location, brain midline, and image intensity and gradient features. The 2D Ce detections are then combined to initialize a 3D active contour that performs the final segmentation. A deformable model approach was also explored by Sridar et al. to segment the Th in [96]. After detecting the head region based on [97], a rigid-affine registration between the image and a reference one containing a model that represents the spacing surrounding the Th is performed, later refining the result using a level-set framework. A template strategy was also proposed by Waechter-Stehle et al. [98] for segmenting multiple structures such as Ce, Th, CSP, and CC. This method initially applies the method of [70] to detect the fetal head location and orientation, later initializing a constructed anatomical model and deforming it to the anatomy through a hierarchical coarse-to-fine deformation approach.

A different segmentation class, ASM (illustration in Fig. 9), was proposed by Gutiérrez-Becker et al. [99]. In this work, a 3D point distribution model (PDM) of the Ce was constructed and used for segmenting this structure by adjusting the model through a genetic algorithm. In [100], an improvement of the method was proposed by replacing the genetic algorithm for a function optimization through a Nelder-Mead simplex search. ASM for Ce segmentation was also proposed by Velásquez-Rodríguez et al. [101,102]. In this method, spherical harmonic functions are used to construct the anatomical model which is optimized during the segmentation process using an intensity-based energy functional [101]. In [102], instead of using gray-level information of the entire image volume, voxel profiles normal to each vertex of the model are used, improving the computational efficiency. In [103], the performance of statistic shape models and active appearance models for Ce segmentation was compared by López and Cosío. In [104], Hermite features were added to the active shape model to improve segmentation accuracy.

Classification techniques were also proposed for brain structures segmentation. Yaqub et al. [105] extended their previous detection method [86] to a segmentation approach. Firstly, the fetal skull position and orientation are estimated as described in [70], estimating a known coordinate space for the entire head and generating rough ROIs for each structure using manually segmented images. Afterward, RF are applied to segment the structure in each ROI using intensity-based and geometric features. In [106], Huang et al. addressed the segmentation of CC and CP, where the method starts by finding regions with homogeneous intensities. The regions are then processed using a region descriptor that character-

Table 4
Overview of brain inner structures analysis methods.

	Reference	Dim.	Structure	Category	Method initialization	Method final stage	UI
Detection	Yaqub et al. [86]	3D	Multi-structures	Learning-based	Feature extraction	RF	A
	Li Y et al. [87]	3D	Multi-structures	Learning-based	Random initial location	Patch-based iterative network	A
	Alansary et al. [88]	3D	Multi-structures	Learning-based	Random initial location	Reinforcement learning	A
	Sofka et al. [89, 90]	3D	Multi-structures	Learning-based	–	Integrated detection network	A
	Huang et al. [79]	3D	Multi-structures	Learning-based	Head detection	View-based projection network	A
	Luo et al. [91]	2D	Multi-structures	Learning-based	–	RPN	A
	Lin et al. [92, 93]	2D	Multi-structures	Learning-based	–	Faster R-CNN	A
	Ramos et al. [94]	2D	Ce	Learning-based		YOLO	A
Segmentation	Annangi et al. [95]	2D	Third ventricle	G.Intensity-based	Skull stripping	Phase analysis and threshold	A
	Liu et al. [30]	3D	Ce	Def. models	Probabilistic boosting tree	Active contours	A
	Sridar et al. [96]	2D	Th	Def. models	Head detection, registration	Distance regularized level set	A
	Waechter-Stehle et al. [98]	3D	Multi-structures	Def. models	Head detection, registration	Template deformation	A
	Gutiérrez-Becker et al. [99,100]	3D	Ce	ASM	Model at defined location	Point distribution model	A
	Velásquez-Rodríguez et al. [101,102]	3D	Ce	ASM	Model at defined location	Spherical harmonic model	A
	López et al. [103,104]	3D	Ce	ASM	Model initialization	Statistic/appearance model	MI
	Yaqub et al. [105]	3D	Multi-structures	Learning-based	Head detection	RF	A
	Huang et al. [106]	2D	Multi-structures	Learning-based	Candidate regions	Boosting classifier	A
	Venturini et al. [107]	3D	Multi-structures	Learning-based	Skull ROI	V-Net	MR
	Maraci et al. [109]	2D	Ce	Learning-based	–	FCN	A

A: Automatic method, MI: semiautomatic method (manual initialization), MR: semiautomatic method (ROI definition).

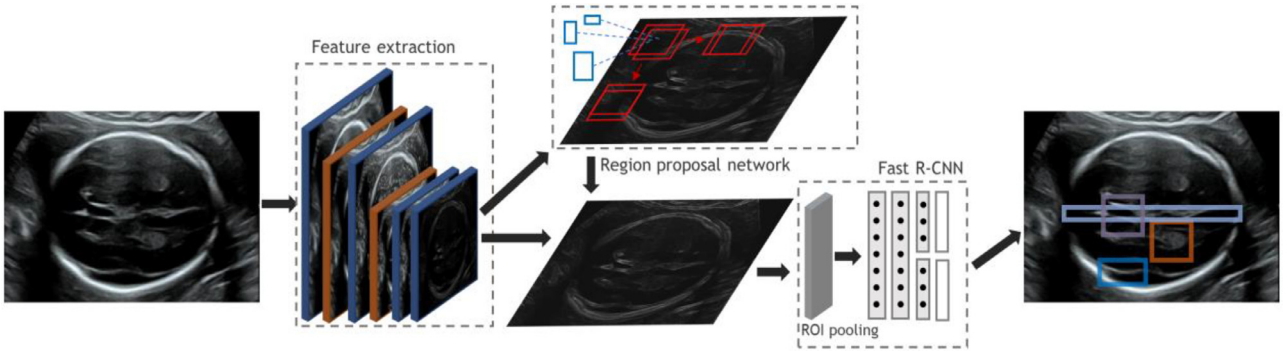

Fig. 8. Detection of brain structures in fetal US using an object detector approach, namely faster R-CNN.

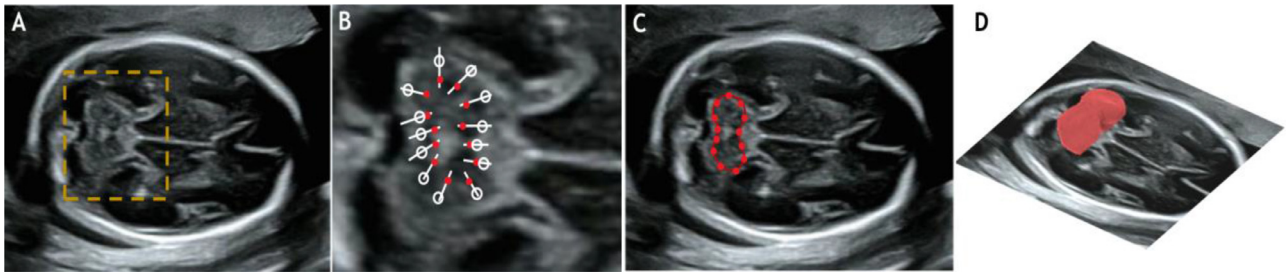

Fig. 9. Illustration of ASM approach to segment the Ce in US images. (A) Original image in the TC plane with the Ce region outlined; (B) Zoomed view of the Ce. The red dots represent a PDM model, the white circles represent the best positions for the PDM model (Ce boundary), and the white lines represent the regions where local appearances are evaluated; (C) Final position of the PDM model and respective final segmentation; (D) 3D representation of Ce.

izes the shape and local intensity, being the descriptor combined with a boost classifier to segment the structures. More recently, DL strategies have been proposed. In [107], Venturini et al. used a V-Net architecture [108] to simultaneously generate segmentation masks of Ce, Th, white matter, and brainstem. In [109], Maraci et al. segmented the Ce using an FCN configuration in 2D US images of the axial TC plane.

5.2. Performance assessment

The performance of the methods for fetal brain structures analysis reviewed in section 5.1 is described in Table 5. For the methods included in the brain structures detection category, the assessment is performed in terms of detector's success, which evaluates the accuracy of the bounding box found for each structure, and in terms of point-based evaluation, which measures the distance between structure landmarks detected automatically and the manual ones. For the segmentation methods, an assessment in terms of region and contour-based analysis is presented, similarly to Table 3. Biometry analysis for the brain structures is also presented in Table 5 when found in the reviewed works. Finally, the same criteria described in Section 4.2 to limit the scope of the comparison between methods was applied.

5.3. Discussion

When analyzing the type of methods proposed in the literature for brain inner structure detection (Table 4), it is possible to verify that learning-based approaches are more frequently used. Structure detection can be performed by detecting a landmark point in the structure or by obtaining a bounding box for the structure region. Due to the speckle noise, unclear structure boundaries, and variation of image appearance, identification of the brain structures is challenging, even by naked-eye evaluation, and so, simple global intensity-based methods are not suitable for either of the detection tasks. In this sense, supervised learning is applied, where besides intensity image information, relative position features such as the interdependence of structures can be added. Indeed, the first works using machine learning for fetal brain structure detection used spatial information to perform the detection. Moreover, a hierarchical scheme was often applied in the early works for brain structures detection, whether using coarse-to-fine detection at different resolution levels or using an iterative approach were the location of the structures is updated at each iteration. This aspect can suggest the difficulty of detecting the brain structures at only one stage in a direct and accurate way. In the recent works, DL-approaches are being used to perform the direct detection of the structures [91–94].

The most recent works proposed to adapt well-known DL object detectors (RPN, R-CNN, YOLO) for structure detection in US images, taking advantage of the fact that this type of detectors has been actively studied in computer vision in recent years, having a well-defined configuration. In fact, these detectors were proposed to combine the region search procedure needed for object detection with CNN features, achieving accurate results. However, these DL models are typically designed to learn from a high number of images and the size of datasets of ultrasound images is typically reduced. This issue is even more heightened by the variable appearance of the fetal brain structures in the US, enhancing the need of a large and bringing issues regarding the use of these DL detectors on such datasets. One solution applied by the works is to use transfer learning to initialize CNN with pretrained weights on non-medical images, allowing to apply the knowledge acquired on other tasks to the problem of structure detection on ultrasound images. However, due to the difference of non-medical and medical images, a robust fine-tuning to the medical imaging task needs to be applied to translate a computer vision task to the medical context.

A more difficult task concerns brain structure segmentation. Here, the topological flexibility of deformable models and ASM was explored in the early works. Besides this type of methods being robust to weak boundaries, they intrinsically incorporate shape information, which is useful to obtain an accurate segmentation of challenging objects. However, the main problem associated with this type of methods is that they require a strong initialization. To provide the initialization for the segmentation methods based on deformable models, a template-based approach is usually performed, where a template that will serve as initial contour is registered with the image to evaluate. However, due to the variable orientation of the fetal head in US imaging, this task is not straightforward. For the ASM-based approaches, a searching procedure using an objective function is usually applied to define the initial position for the statistical model. However, such approach is suboptimal and highly dependent on the correct alignment, which can lead to a misleading position due to the low quality of the US image. Traditional machine learning techniques were also applied for fetal brain structure segmentation, and similarly to the methods for detection tasks, region descriptors and position features were used in the methods. In the latest state-of-the-art, DL methods are being explored.

Overall, by analyzing the works proposed for both tasks, i.e., structure detection and segmentation, it is possible to verify that DL approaches are now been used to supersede the state-of-the-art methods. However, most of the methods are applying already described networks for detection or segmentation. Despite this type of strategy is leading to good results, for the authors' point-of-view the integration of other type of information in the learning approach (e.g. global shape or anatomical correspondences) can potentiate even more the accuracy of the methods and should be analyzed by the research field.

6. Standard anatomical plane analysis

6.1. Overview of methods

Detection of standard anatomical planes of the fetal brain during US examination is crucial to assess anatomic integrity and extract biometric data. The traditional practice relies on the manual identification of standard planes. However, its accurate identification is a challenging task highly dependent on the sonographer's expertise. Two different types of approaches were proposed in the literature to automate this task. The first one relies on plane detection in a 3D US volume. The second one is a classification approach to confirm if a 2D US image corresponds to a standard plane. Table 6 summarizes the methods presented in the state-of-the-art for both approaches.

6.1.1. Standard head plane detection methods

Some works reviewed in Sections 4 and 5 had as the final goal the detection of standard anatomical planes from 3D US volumes. In the work of Sofka et al. [90], the planes were automatically estimated after brain structures detection. Instead of retrieving the planes directly from detected brain structures, other works proposed different strategies. In the work of Cuingnet et al. [70], it was also addressed the task of MS plane detection. For that, a global intensity-based approach was performed to estimate the rotation angle that must be applied to transform a plane previously generated using head and eyes information in the MS plane, using a weighted HT transform. A deformable models was explored by Namburete et al. [110], where a template model with the reference planes (TC, TT and TV) is deformed to the target anatomy. Thus, during the template deformation, the planes are also transformed

Table 5
Performance assessment of brain structures analysis methods.

Reference	N	GA (week)	Detector/Region evaluation		Point/Contour evaluation		Biometry evaluation	
			Metric	Value	Metric	Value	Metric	Value
Yaqub et al. [86]	10	19–24	PR_{CP}, RE_{CP}, AC_{CP}	86.0, 83.4, 92.9%	–	–	–	–
			PR_{PVC}, RE_{PVC}, AC_{PVC}	74.3, 73.8, 91.1%				
			PR_{CSP}, RE_{CSP}, AC_{CSP}	68.8, 76.3, 91.9%				
			PR_{CER}, RE_{CER}, AC_{CER}	64.4, 72.4, 91.9%				
Li et al. [87]	22	–	–	–	PD_{mean}	5.59 ± 3.09 mm	–	–
Alansary et al. [88]	21	–	–	–	$PD_{R\text{-}CER}$	2.37 ± 0.86 mm	–	–
					$PD_{L\text{-}CER}$	2.73 ± 1.38 mm		
					PD_{CSP}	3.66 ± 2.11 mm		
Sofka et al. [89]	107	16–35	–	–	PD_{CER}	3.09 ± 1.71 mm	–	–
					PD_{CC}	4.20 ± 2.13 mm		
Sofka et al. [90]	108	16–35	–	–	PD_{CER}	1.75 ± 0.92 mm	ME_{CER}	1.37 ± 1.10 mm
					PD_{CM}	1.95 ± 0.93 mm	ME_{CM}	0.87 ± 0.58 mm
					PD_{LV}	1.72 ± 0.93 mm	ME_{LV}	1.01 ± 0.7 mm
					PD_{CC}	1.89 ± 0.96 mm		
					PD_{CP}	1.83 ± 0.78 mm		
Huang et al. [79]	45	20–29	IOU_{CSP}	63.2 ± 15.2%	PD_{CSP}	1.8 ± 1.5 mm	ME_{CER}	1.5 ± 0.7 mm
			IOU_{LV}	48.7 ± 19.1%	PD_{LV}	2.4 ± 2.0 mm	ME_{CM}	2.0 ± 0.9 mm
			IOU_{Th}	68.1 ± 14.7%	PD_{Tha}	1.9 ± 1.7 mm		
			IOU_{CER}	66.5 ± 14.6%	PD_{CER}	2.0 ± 1.9 mm		
			IOU_{CM}	65.9 ± 15.3%	PD_{CM}	2.1 ± 1.9 mm		
Luo et al. [91]	265	20–24	IOU_{TVe}	86.12%	–	–	–	–
			IOU_{BM}	98.87%				
			IOU_{Th}	94.21%				
			IOU_{CP}	93.76%				
			IOU_{CSP}	95.57%				
			IOU_{LS}	97.92%				
Lin et al. [92]	1153	14–28	PR_{LS}, RE_{LS}	96.6, 96.8%	–	–	–	–
			PR_{CP}, RE_{CP}	96.7, 96.0%				
			PR_{Th}, RE_{Th}	77.1, 89.6%				
			PR_{CSP}, RE_{CSP}	94.6, 89.3%				
			PR_{TV}, RE_{TV}	72.8, 56.5%				
Lin et al. [93]	320	14–28	IOU_{TV}	82.50%	–	–	–	–
			IOU_{BM}	98.95%				
			IOU_{Th}	93.89%				
			IOU_{CP}	95.82%				
			IOU_{CSP}	89.92%				
			IOU_{LS}	98.46%				
Ramos et al. [94]	78	–	PR_{CER}, $F1_{CER}$	66, 100%	–	–	–	–
Liu et al. [30]	14	20–33	$DICE_{CER}$	84%	–	–	–	–
Sridar et al. [96]	100	18–20	SP_{Th}, DSC_{Th}	77 ± 3, 74 ± 3%	HD_{Th}	1.06 ± 0.17 mm	ME_{Th}	16.74 ± 1.95 mm
Gutiérrez-Becker et al. [100]	20	18–24	DSC_{CER}	80 ± 4.6%	–	–	–	–
Velásquez-Rodríguez et al. [102]	10	–	DSC_{CER}	75.44 ± 5.21%	–	–	–	–
Velásquez-Rodríguez et al. [101]	10	–	DSC_{CER}	68.90 ± 2.69%	–	–	–	–
Yaqub et al. [105]	20	18–26	DSC_{CP}, VD_{CP}	79 ± 9%,	–	–	–	–
			DSC_{PVC}, VD_{PVC}	-25 ± 26mm^3				
			DSC_{CSP}, VD_{CSP}	82 ± 10%,				
			DSC_{CER},VD_{CER}	1 ± 32mm^3				
				74 ± 11%,				
				7 ± 10mm^3				
				63 ± 15%,				
				2 ± 14mm^3				
Huang et al. [106]	52_{CP}	20–30	AC_{CP}, RE_{CP}, SP_{CP},	99.4, 97.2,9.6,	HD_{CP}	7.7 ± 3.4 mm	ME_{CP}	6.7 ± 4.5 mm
	82_{CC}		PR_{CP}	94.5%	HD_{CC}	2.80 ± 1.91 mm	ME_{CC}	1.81 ± 1.40 mm
			AC_{CC}, RE_{CC}, SP_{CC},	98.0, 94.7, 98.6,				
			PR_{CC}	97.6%				
Venturini et al. [107]	48*	20–25	DSC_{TH}	81.1 ± 6.1%	HD_{Th}	3.80 ± 1.95 mm	–	–
			DSC_{BS}	82.0 ± 8.1%	HD_{BS}	4.14 ± 1.29 mm		
			DSC_{CER}	77.3 ± 14.9%	HD_{CER}	4.20 ± 2.39 mm		
			DSC_{WM}	92.1 ± 3.3%	HD_{WM}	5.93 ± 2.28 mm		
Maraci et al. [109]	3236	16–26	AC_{CER}, IOU_{CER}	86.99, 81.62%	–	–	–	–

N: number of images; AC: accuracy, AUC: DSC: Dice similarity coefficient, F1: F1-score, IOU: intersection over union, PR: precision, RE: recall, SP: specificity; HD: Hausdorff distance, PD: point/landmark distance; ME: mean error. *INTERGROWTH-21st data.

to the optimal location in the target patient. An illustration of this concept is presented in Fig. 10. A similar concept was applied by Waechter-Stehle et al. [98]. Nevertheless, to solve potential inconsistences caused by manual annotations variability, a learning-based solution to correctly estimate the optimal plane definition based on annotations was applied.

In [111], a machine learning approach based on RF was proposed by Yaqub et al. for PS plane detection. Informative voxels were located using a phase-based approach and their strength was used to weight their contribution throughout the training. Plus, geometric features retrieved from a manually located MS plane are added to the RF framework, being the output of the method the parameters of the PS plane. This method was improved in [52], automating the MS plane identification based on the head skull and its midline using HT. Another machine learning approach was implemented by Li Y et al. for TC and TV detection [112]. The method

Table 6
Overview of standard anatomical planes analysis methods.

	Reference	Plane	Category	Method initialization/requirements	Method description	UI
Detection	Sofka et al. [90]	Multi-plane	–	Structure detection by integrated detection network	Retrieved from structures	A
	Cuingnet et al. [70]	MS	G. Intensity-based	Head and eyes detection, plate detector	Weighted HT	A
	Namburete et al. [110]	Multi-plane	Def. models	Surface initialization with planes	Template deformation	MI
	Waechter-Stehle et al. [98]	Multi-plane	Learning-based	Head detection and template/plane deformation	Annotations learning	A
	Yaqub et al. [52, 111]	PS	Learning-based	Phase-based analysis and detection of MS plane	RF	MI /A
	Li Y et al. [112, 113]	Multi-plane	Learning-based	Random plane initialization	CNN	A
Classification	Yaqub et al. [73]	TV	Score-based	Head detection, CNN symmetry and CSP analysis	CNN	A
	Lin et al. [92,93]	TT	Score-based	Brain structures detection	R-CNN	A
	Luo et al. [91]	TT	Score-based	Brain structures detection	Class prediction network	A
	Zhang et al. [115]	No defined	Score-based	Head and falx detection and feature extraction	RF	A
	Yaqub et al. [116]	Multi-plane	Score-based	Head ROI detection and feature extraction	RF	A
	Liu et al. [117]	TT	Score-based	Head detection and ASM fitting	Discriminative analysis	A
	Kim et al. [46]	TT	Score-based	Head detection and image alignment	CNN	MI
	Maraci et al. [109]	TC	Learning-based	Image directly applied	CNN	A
	Qu et al. [118]	Multi-plane	Learning-based	Image directly applied after head ROI crop	CNN with transfer learning	MR
	Qu et al. [119]	Multi-plane	Learning-based	Image directly applied	Differential CNN	A
	Baumgartner et al. [23,24]	Multi-plane	Learning-based	Image directly applied	CNN/SonoNet	A
	Schlemper et al. [120]	Multi-plane	Learning-based	Image directly applied	SonoNet with attention unit	A

A: Automatic method, MI: semiautomatic method (manual initialization), MR: semiautomatic method (ROI definition).

was denominated iterative transformation network, where a CNN was used to learn the mapping between a plane and the transformation needed to move the plane towards the standard plane in the US volume. An iterative approach was used, where the CNN is used at each iteration to improve plane location. Later, the same authors added additional classification probability outputs as confidence measures of the transformation parameters to improve the results [113].

6.1.2. Standard head plane classification methods

Strategies to evaluate the quality of a 2D view, i.e. if an 2D image corresponds to one standard anatomical plane, were also proposed in the literature. In these methods, it is verified if the view satisfies clinical anatomical constraints. For that, several methods compute a score for a US view based on factors such as presence of certain anatomical structures, head appearance/shape, or brain symmetry properties [114]. In [92], Lin et al. targeted the identification of TT plane by first detecting several anatomical structures and then attributing a score to each detected structure, consequently estimating the quality of the plane. In [93], besides scoring the detected structures, it was also verified the fetal skull shape, confirming if it occupies the sufficient image area to meet clinical standards. The work of Luo et al. [91] was also focused on TT plane evaluation. However, instead of scoring based on detected anatomies, a class prediction network integrated into the multi-task detection architecture is used to confirm if the structures present the required clinical standards. Other authors did not explicitly detect the brain structures to perform plane quality assessment. For example, in the work of Zhang et al. [115], head appearance was analyzed for image quality assessment. For that, the previously proposed method [58] is firstly used to extract the head region and HT is applied to detect its midline falx. Head appearance, shape, and midline features are then extracted and integrated into a RF classifier to grade the image into good or poor image quality. RF were also used by Yaqub et al. in [116] to distinguish TV and TC planes, along with other fetal planes. Here, ROI detection is initially performed to detect the head and other fetal body structures, using a similar approach to [52]. Features invariant to translation and orientation are then extracted from the obtained ROI's and used in the RF framework to categorize the fetal image. Liu et al. [117] classified the TT plane by firstly detecting head position and orientation using the method of [49]. Afterward, an ASM head model is fitted to the image to capture a butterfly-like shape, representing the appearance of the Th, CSP, and midline falx. After fitting, a learning-based approach based on linear discriminative analysis is applied to calculate the probability of the image corresponds to the TT plane. Examination of CSP, Th, and midline falx was also studied by Kim et al. in [46], together with the evaluation of Ce's absence. Here, after head detection and image alignment using prior anatomical information, a CNN is applied to evaluate the image, scoring each parameter evaluated. Yaqub et al. [73] used a CNN-based approach to score the TV plane using information retrieved from the segmented head, symmetric/asymmetric anatomical patterns, and CSP visibility. A CNN was also applied by Maraci et al. [109] to directly classify an image as TC plane or otherwise. The same concept was applied by Qu et al. in [118], where a transfer-

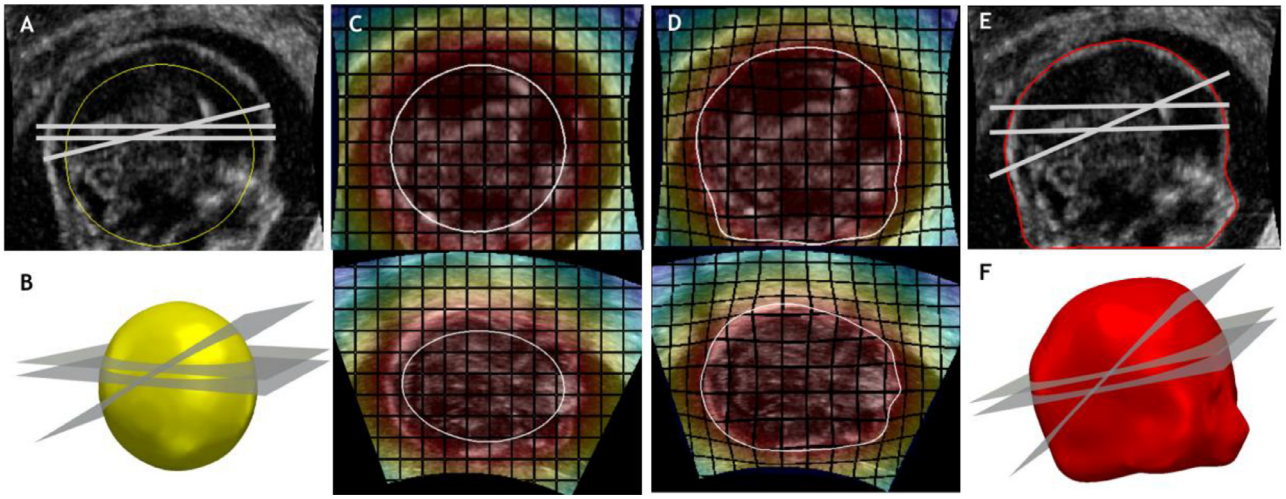

Fig. 10. Illustration of a template deformation approach to segment the fetal head and detect standard anatomical planes during the deformation process. (A) US image with a contour representation of the template model in yellow and respective standard anatomical planes; (B) 3D view of the template model with the planes; (C) Two views of the US image with the initial template; (D) Contour representation after applying global and local deformation to the template model. (E) Final contour representation after template deformation approach and new planes detected using the same transformation found for the head model; (F) 3D view of the final model.

learning CNN approach was proposed to classify a US image in six different categories, namely: TV, TT, TC, MS, PS, and coronal TV. In [119], the same team used a differential-CNN for brain planes classification. In [23], a CNN-based approach was also applied by Baumgartner et al. to classify in real-time TV and TC planes, along with other body fetal planes. A more complex very deep network architecture, denominated SonoNet, was implemented in [24] to improve classification accuracy. Finally, Schlemper et al. [120] proposed to incorporate self-gated soft-attention mechanisms into the SonoNet architecture, allowing the network to contextualize local information for improvement of the detection.

6.2. Performance assessment

Evaluation of standard anatomical plane analysis methods is shown in Table 7. Here, the performance is evaluated by measuring the errors of the detected planes and by analyzing the classification accuracy of image quality assessment.

The performance evaluation of the methods for anatomical standard plane detection is highly variable. Indeed, when assessing head/brain structures segmentation or detection methods, well-established state-of-the-art metrics can be used. However, common metrics to quantify plane detection are lacking in the literature. Thus, once the variance of plane position and orientation is difficult to interpret, different evaluation approaches were followed by the multiple teams. In [90], the plane error was computed as the distance between the endpoints of two lines that represent the detected and manual 2D planes. In [110], dihedral angles calculated using the normal vectors of the planes were used to quantify plane errors. Plus, distance errors were also evaluated by extracting points on the cranial contour in the detected plane and computing the average Euclidean distance between these points and the ones on the manual plane. In [52,98,111-113], dihedral angles were also used, but the distance plane errors were given by the Euclidean difference between the center of the planes. Plus, in [112,113], image similarity of the planes is also measured using the peak signal-to-noise ratio (PSNR) and structural similarity (SSIM). Concerning the methods that perform classification of standard anatomical planes, few proposed to evaluate each parameter used to classify the image, instead of evaluating the final classification result [73,92,93].

6.3. Discussion

Concerning standard anatomical planes detection, methods with this finality are very important in clinical practice to avoid time-consuming manual detection in 3D volumes during the sonographic examination. Here, several automatic approaches were researched. Three main types of approaches seem to be interesting for plane detection. The first one consists of detecting brain structures and using their location to generate a plane that is feasible to be used to evaluate the structure or use the location of different structures to retrieve the standard anatomical plane that includes them. The second approach consists of to embed plane information in a head shape model, which is afterward used to segment the head on a deformation process, which is also applied to the planes to find their new location/orientation. The third one uses a learning-based approach to estimate the transformation that should be applied to an initial plane to obtain the ideal anatomical plane. As different as the approaches may seem, all of them showed to be feasible to be used in this ambit. Interestingly, in the literature, no work exploited the main advantages of the three main types, combining them to improve the overall method's performance for plane detection. Indeed, using a DL approach to iteratively find the transformation to be applied to a random initial plane seems to be a good strategy, but can be sensitive to the initial plane. Thus, from the authors' perspective, using a template-based approach to find an initial plane closer to the real one can be an elegant solution. Moreover, integrating information of the brain structures present in the transformed plane at each iteration can potentially increase the robustness of the plane detection. Another aspect that should be noted is that no work was found to directly retrieve the plane parameters from the image using a DL approach. Here, a regression-based CNN could be an option to estimate the plane parameters. Moreover, different tasks can be integrated into the network (e.g. structures detection or segmentation) to try to potentiate the parameter estimation.

Still concerning standard anatomical analysis, methods that assess image quality (i.e. if a 2D image corresponds to a specific plane) were also proposed. Here, two different approaches were used. The first one consists of evaluating clinical criteria, such as presence/absence of structures, symmetry, and image appearance, to verify if an image corresponds to a standard plane. These parameters are often evaluated using a learning-based approach,

Table 7
Performance assessment of standard plane evaluation methods.

Reference	N	GA (weeks)	Plane detector evaluation/ Classification evaluation	
			Metric	Value
Sofka et al. [90]	108	16–35	$PME_{CER-PLANE}$	2.81 ± 1.24 mm
			$PME_{CM-PLANE}$	2.30 ± 0.96 mm
			$PME_{LV-PLANE}$	2.21 ± 0.98 mm
Namburete et al. [110]	52	18–28	DA_{TC}, PME_{TC}	1.5 ± 8.4°, 4.31 ± 1.79 mm
			DA_{TT}, PME_{TT}	0.8 ± 6.6°, 3.55 ± 1.58 mm
			DA_{TV}, PME_{TV}	2.6 ± 7.3°, 4.63 ± 1.91 mm
Waechter-Stehle et al. [98]	14	–	DA_{TC}, PME_{TC}	4.71 ± 2.18°, 1.20 ± 0.68 mm
Yaqub et al. [111]	43*	23–27	DA_{PS}, PME_{PS}	9.0 ± 4.3°, 8.3 ± 3.1 mm
Yaqub et al. [52]	161	23–33	DA_{MS}, PME_{MS}	5.6 ± 2.6°, 2.1 ± 1.9 mm
			DA_{PS}, PME_{PS}	10.3° ± 3.7°, 10.2 ± 4.0 mm
Li et al. [113]	22	–	DA_{TV}, PME_{TV}, $PSNR_{TV}$, $SSIM_{TV}$	10.7 ± 5.7°, 3.49 ± 1.81 mm,
			DA_{TC}, PME_{TC}, $PSNR_{TC}$, $SSIM_{TC}$	16.6 ± 1.8, 0.413±0.082
				11.4 ± 6.3°, 3.39 ± 2.13 mm,
				16.8 ± 2.1, 0.437±0.110
Li et al. [112]	22	–	DA_{TV}, PME_{TV}, $PSNR_{TV}$, $SSIM_{TV}$	12.4 ± 12.8°, 3.45 ± 1.73 mm,
				16.5 ± 1.9, 0.418±0.080
Yaqub et al. [73]	19,838	–	AC_{head}	94.1%
			$AC_{symmetry}$	83.1%
			$AC_{CSP-visibility}$	86.8%
Lin et al. [92]	1153	14–28	RE_{TV}, PR_{TV}, AC_{TV}	56.5,72.8, 44.1%
Lin et al. [93]	320	14–28	RE_{TT}, PR_{TT}, AC_{TT}, $F1_{TT}$, SP_{TT}, AUC_{TT}	93.57, 97.76, 96.25, 95.62, 98.33,
				98.84%
Luo et al. [91]	265	20–24	RE_{TT}, PR_{TT}, AC_{TT}, $F1_{TT}$, SP_{TT}, AUC_{TT}	94.73, 96.71, 93.32, 95.91, 94.49,
				95.67%
Zhang et al. [115]	21	20–35	AC, RE, SP	95.24, 87.5, 100%
Yaqub et al. [116]	29,858	18–22	AC_{mean}	75%
Kim et al. [46]	70		K	0.53
Maraci et al. [109]	1000	16–26	RE_{TC}, PR_{TC}, AC_{TC}	99, 99, 99%
Qu et al. [118]	240	–	RE_{mean}, PR_{mean}, AC_{mean}, $F1_{mean}$	89.1, 85.0, 86.4, 90.1
Qu et al. [119]	19,142	16–34	RE_{mean}, PR_{mean}, AC_{mean}, $F1_{mean}$	92.39, 92.62, 93.11, 93.53%
Baumgartner et al. [23]	201	18–22	RE_{TV}, PR_{TV}	96, 90%
			RE_{TC}, PR_{TC}	92, 94%
Baumgartner et al. [24]	539	18–22	RE_{TV}, PR_{TV}	98, 86%
			RE_{TC}, PR_{TC}	96, 90%
Schlemper et al. [120]	38,243	18–22	RE_{TV}, PR_{TV}, $F1_{TV}$	99.0, 98.0, 98.5%
			RE_{TC}, PR_{TC}, $F1_{TC}$	98.2, 98.8, 98.5%

N: number of images; AC: accuracy, AUC: area under curve, DA: dihedral angle, F1: F1-score, K: Cohen's kappa, PME: plane mean error, PR: precision, RE: recall, SP: specificity. *INTERGROWTH-21st data.

scoring multiple parameters to perform a quality assessment of the image. The second approach relies on a learning-based method, namely DL, that poses plane assessment as a classification problem, where the US image is directly fed to a network that categorizes the image. On one hand, the classification can be binary, where the network categorizes the image with a label if it corresponds to a specific plane or with another label if otherwise. On the other hand, a multi-class classification approach can be used, where different labels are assigned to the images according to the plane that they represent. Here, similarly to plane detection, the integration of structure detection or segmentation tasks in the DL-approach can be studied to increase the classification accuracy.

7. Fetal head development analysis

7.1. Overview of methods

Fetal biometric parameters such as HC, BPD, and OFD are monitored in obstetrics to evaluate head fetal development. An overview of methods that used these parameters for fetal developmental analysis is presented in Table 8. This section is divided into two parts. Firstly, methods that aim to estimate GA, which is daily performed to monitor the fetal head growth, are presented. Secondly, methods that classify a fetus as normal or abnormal are described.

7.1.1. Gestational age prediction

Despite the last period of the mother can be used to predict GA at the beginning of the pregnancy, the clinical recommendation for the first trimester is to use crown-rump length (from the head to the buttocks) for the estimation. However, in advanced weeks of pregnancy, head biometry parameters, that can be estimated by image processing methods, are used for GA estimation, using a simple statistical method. Here, analysis of standard tables or charts that correlate biometric parameters with GA is included. This simple approach was used by Marhaban et al. [31], Annangi et al. [95], and Saii and Kraitem [32], where BPD was used to estimate GA. In the works of Rahayu et al. [48] and Imaduddin et al. [37], the authors also added the femur length (FL) measurement to improve the GA estimation. Instead of BPD, HC was used by Banerjee and Krishnan [49] and Heuvel et al. [59]. In [109], Maraci et al. used the Transcerebellar diameter to estimate GA, claiming that this parameter is least likely to be affected by fetal growth disturbances, being more suitable for GA estimation. In [41], Cerrolaza et al. proposed to use a 3D-based measurement, instead of the traditional 2D biometric parameters, to avoid the subjectivity in 2D diagnostic plane selection for biometry estimation. Thus, the semi-axis of a segmented 3D model of the skull was processed by a linear regression method for GA prediction. In [121], a more complex method for GA and brain maturation estimation was proposed by Namburete et al. In this method, instead of using directly biometric measurements, brain appearance in the image was evaluated in an RF framework. Firstly, the method proposed in [69] is used for

Table 8
Overview of fetal development analysis methods.

	Reference	Dim.	Parameters	Category	Method description
Age estimation	Marhaban et al. [31]	2D	BPD	Statistics	Standard table analysis
	Annangi et al. [95]	2D	BPD	Statistics	Standard table analysis
	Saii and Kraitem [32]	2D	BPD	Statistics	Standard table analysis
	Rahayu et al. [48]	2D	BPD and FL	Statistics	Standard table analysis
	Imaduddin et al. [37]	2D	BPD and FL	Statistics	Standard table analysis
	Banerjee and Krishnan [49]	2D	HC	Statistics	Standard table analysis
	Heuvel et al. [59]	2D	HC	Statistics	Chart analysis
	Maraci et al. [109]	2D	Transcerebellar diameter	Statistics	Mathematical relation
	Cerrolaza et al. [41]	3D	3D skull axis	Statistics	Linear regression model
	Namburete et al. [121,122]	3D	Image, local size, HC	Learning-based	RF
Abnormality detection	Gadagkar and Shreedhara [67]	2D	HC, AC	Machine learning	ANN
	Rawat et al. [65]	2D	HC, AC	Machine learning	ANN
	Sahli et al. [123]	2D	BPD, AC, HC	Machine learning	SVM
	Sahli et al. [29,124]	2D	Texture/Texture and geometry	Machine learning	SVM/PCA+ANN
	Xie et al. [74]	2D	Image	Machine learning	CNN

skull stripping and to sample anatomical brain regions where patterns of fetal brain changes can be learned. Then, bespoke features, namely appearance, local size, and HC, are integrated into the RF method to estimate GA and the neurodevelopmental stage of a fetus. In [122], an extension of the method was presented, adding unary, sulcal, and Haar features.

7.1.2. Abnormality classification

Early detection of fetal abnormality using US examination is a complex task, due to poor image quality. Thus, methods that classify a fetus as normal or abnormal have been researched. Intrauterine growth restriction (IUGR), typically associated with low fetal weight, is frequently searched. Artificial neural networks (ANN) were used by Gadagkar and Shreedhara [67] and Rawat et al. [65] to classify a fetus as normal or abnormal concerning IUGR, using HC and abdominal circumference (AC) parameters. Besides fetal growth analysis, automatic methods to detect abnormalities in the fetal brain and head are needed. In [123], SVM was used by Sahli et al. to distinguish normal and abnormal head shape using BPD, OFD, and HC. Here, abnormal conditions include dolichocephaly and microcephaly. Hydrocephaly was addressed by the same team in [124], where a SVM was used to evaluate image appearance. Once this pathology is related to fluid accumulation inside the ventricles, image appearance differs from normal ones. In [29], geometrical features were also added to enhance hydrocephalus characterization, where a feature reduction by PCA and ANN for classification are combined for the classification. In [74], Xie et al. proposed a method to detect fetal CNS malformations. A CNN that directly analyzes the US image of the fetal brain and classifies the image as normal or abnormal is used in this work. Plus, a heat map for lesion localization is also obtained by the CNN, allowing to locate lesions such as cysts, intracranial hemorrhage, or other conditions.

7.2. Performance assessment

The performance of the methods proposed for fetal development analysis is presented in Table 9, where the difference between the automatic and manual estimation of GA is presented along with the errors of fetal abnormality classification.

7.3. Discussion

Regarding the methods for fetal development analysis (Table 8), it can be verified that most of them perform GA estimation and abnormality analysis by comparing automatic biometric measurements with the ideal ones. Here, several methods consider the values presented in [125] as the reference values. However, only a few methods used image information to evaluate fetal abnormality. Despite fetal condition evaluation in the traditional clinical practice being preferably performed through biometric measurements, particularly for IUGR, evaluation of the image appearance can bring additional information that can be relevant to detect pathologies. Specifically, there are pathologies that can be diagnosed using image information instead of using only biometric indexes, such as holoprosencephaly, encephalocele, or spinal dyspraphism (please see Section 2.2). Nevertheless, no work was found to address the diagnosis of this type of pathologies. Moreover, methods to address the detection and evaluation of destructive lesions (*e.g.* tumors or cysts) are also lacking in the literature. Here, automated methods to segment these lesions can revolutionize the clinical practice, allowing the quantification of these lesions and enabling an accurate monitorization of a fetus with this type of conditions.

8. Image processing enhancement

8.1. Overview of methods

As stated before, processing of fetal US images is not a straightforward task due to image quality and presence of shadows, which can occlude some relevant anatomies. Moreover, due to the reduced field-of-view (FOV) of US, partial head acquisitions are common. Thus, methods to ease the interpretation or to enhance the information of US images were proposed. These methods include head referential estimation, US compounding, and registration approaches. An overview of these methods is presented in Table 10.

8.1.1. Head *referential estimation*

Since US acquisition relies on the free-hand manipulation of a probe, fetal brain position and orientation are highly variable, hampering the development of automatic method solutions. Thus, some teams explored strategies to estimate a referential anatomical cartesian. Cuingnet et al. [70] estimated this referential based on information retrieved from the previously described technique to detect the skull, eyes, and MS plane. In [126], Namburete et al. researched a DL for this task. Here, a multi-task FCN was used to derive fetal brain orientation, eye localization, and brain extraction, consequently estimating the transformation matrix that aligns the fetal head to a common coordinate space.

8.1.2. US compounding and reconstruction methods

One problem associated with the head fetal examination is that the US imaging system can present a small FOV that can hamper full fetus head acquisitions, mainly at the end of gestation. Another problem is that shadows and artifacts present in the US images

Table 9
Performance assessment of fetal development analysis methods.

Reference	N	GA	Metric	Value
Marhaban et al. [31]	20	14–38	ME_{GA}	0.49 – 8.49 days
Rahayu et al. [48]	30	15–25	AC_{GA}	97.77%
Imaduddin et al. [37]	50	–	ME_{GA}	0.5%
Heuvel et al. [59]	335	–	$ME_{1st\text{-}GA}$	0.6 ± 4.3 days
			$ME_{2nd\text{-}GA}$	0.4 ± 4.7 days
			$ME_{3rd\text{-}GA}$	2.5 ± 12.4 days
Cerrolaza et al. [41]	10	20–30	ME_{GA}	0.5 ± 0.3 weeks
Namburete et al. [121]	130	18–27	ME_{GA}	4.62 days
Namburete et al. [122]	157	18–33	$ME_{2nd\text{-}GA}$	5.18 ± 0.97 days
			$ME_{3rd\text{-}GA}$	7.77 ± 0.83 days
Rawat et al. [65]	12	12–34	TE_{IUGR}	−0.047 - 0.387
Sahli et al. [123]	86	17–27	$RE_{Abnormal}$	92.36%
			$SP_{Abnormal}$	84.03%
			$AC_{Abnormal}$	87.10%
Sahli et al. [124]	10	20–22	$RE_{Hydrochepaly}$	91.84%
			$SP_{Hydrochepaly}$	94.77%
			$AC_{Hydrochepaly}$	91.80%
Sahli et al. [29]	10	19	$ME_{Hydrochepaly}$	3.3 ± 0.5%
Xie et al. [74]	4739	18–32	$RE_{Abnormal}$	96.9%
			$SP_{Abnormal}$	95.9%
			$AC_{Abnormal}$	96.31%

AC: accuracy, RE: recall, SP: specificity, ME: mean error, TE: target error.

Table 10
Overview of image enhancement methods.

	Reference	Dim.	Category	Requirements	Method description	UI
Ref.	Cuingnet et al. [70]	3D	G. Intensity-based	Brain extraction, eye location, MS detection	HT and RF	A
	Namburete et al. [126]	3D	Learning-based	Brain extraction, eye location, brain pose	Multi-task FCN	A
Compound	Perez-Gonzalez et al. [127]	3D	Learning-based	Manual registration of volumes	Weight estimation by SVM	MI
	Wright et al. [128]	3D	Registration	Iterative spatial transformer network	Averaging, groupwise registration	A
	Cerrolaza et al. [129]	3D	Learning-based	Skull segmentation	TL-Net and CVAE	MI
	Cerrolaza et al. [130]	2D	Learning-based	Manual skull segmentation	CVAE	MI
Registration	Perez-Gonzalez et al. [42,43]	3D	Registration	SVM/RF for skull and weight estimation	Weighted CPD	A
	Fathima et al. [131]	2D	Registration	HC annotations and phase-based analysis	Phase-based registration and fusion	MI
	Namburete et al. [132]	3D	Registration	Head alignment and phase-based analysis	Multi-channel groupwise Demons	A
	Kuklisova-Murgasova et al. [133–135]	3D	Registration	Atlas-based segmentation of MR	NCC/Block matching	A
	Wright et al. [136]	3D	Learning-based	–	LSTM spatial co-transformer	A

A: Automatic method, MI: semiautomatic method (manual initialization).

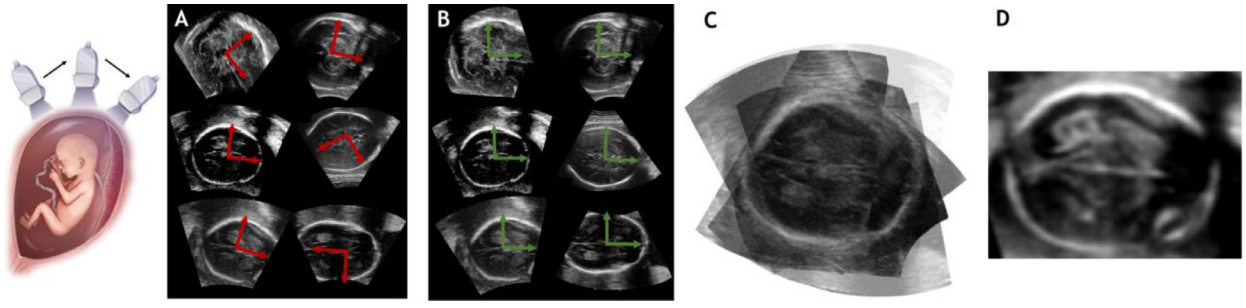

Fig. 11. Illustration of US compounding method. (A) US images acquired from different views; (B) Correction of image orientation using head pose (e.g. estimated manually or automatically); (C) Superposition of the aligned images; (D) Final enhanced US image resulting from (C).

can lead to acoustic occlusions that result in only partially visible fetal head and brain structures. One possible solution to mitigate these issues is the compounding of multiple US volumes of the same patient to create an enhanced volume (Fig. 11). In [127], Perez-Gonzalez et al. proposed a new spatial composition method to fuse multiple US fetal brain projections in a single volume. After registering all the volumes manually, a probabilistic spatial compounding is applied, where weights are estimated for each voxel of each volume, using an SVM that evaluates spatial histogram and texture features. The weights are then used to attribute to each

voxel of the final volume the intensity that best represents the underlying anatomy. In the work presented by Wright et al. in [128], a strategy to fuse US images where the fetal head is only partially visualized is proposed. Here, an iterative spatial transformer network firstly aligns US images from different views to a canonical reference. Then, the different US images are fused by averaging the most salient features from all images, being the compounding image iteratively refined afterward by a group-wise registration approach with the multiple views.

Instead of US compounding, Cerrolaza et al. [129] reconstructed the fetal skull from partially occluded 3D US volumes. The skull is first segmented in the incomplete volume [41]. Then, using the partial segmentation, two networks were compared for skull reconstruction: TL deep convolutional network (TL-Net) and a conditional variational autoencoder (CVAE), which are used to map the occluded volume to the corresponding complete skull. In [130], the 3D fetal was reconstructed from 2D US images of standard anatomical planes, where a reconstruction architecture CVAE directly integrates the three US standard planes as conditional variables for learning a representation of the skull while guaranteeing anatomical consistency.

8.1.3. US registration methods

As can be noticed from the methods of the previous subsection, to create a patient-specific enhanced image of the fetal head and brain structures, the different US acquisitions must be aligned. Thus, some methods addressed the problem of registration of multiple US volumes from the same patient. The method proposed by Perez-Gonzalez et al. in [42] starts by segmenting the skull in each US image. From the segmentation process, point-clouds of the fetal head are generated and registered using a Coherent Point Drift (CPD) method that is used to align sets of points by maximizing the posterior probability between them. However, in this method, a weighted version of the CPD is used, where weights trained by SVM using image features are integrated into the probability estimation. In [43], the SVM classifier was replaced with RF that estimates the weights using features composed of intensity, texture, and edge information. Once known the best alignment between different skull segmentations, aligned US volumes are obtained, which can be posteriorly fused for image enhancement.

Other works addressed the registration of US brain images from different patients. This type of approaches can be useful for comparing different fetuses or to construct a head model representative of a population. A phase-based approach to guide registration of 2D US images was proposed by Fathima et al. [131]. Firstly, a rigid registration using manually annotated skull ellipses is performed to place the images in the same reference space. Local phase analysis is then applied to characterize the image and to guide affine registration with normalized mutual information as the similarity parameter. After registration of the images, a probabilistic US atlas of the fetal brain was constructed by performing wavelet-based image fusion and averaging. Fetal brain atlas construction was also addressed in the work of Namburete et al. [132]. Here, phase analysis is also integrated into the registration process which is achieved by a multi-channel groupwise Demons registration. In this registration approach, an additional channel with phase-based features is added to the intensity image. After registration, the brain atlas can be created by image fusion.

8.1.4. Multimodal registration methods

Despite US being the primary screening modality for fetal evaluation, high quality Magnetic Resonance (MR) imaging (Fig. 12) can be used to improve soft tissues analysis or to confirm pathologic cases. Thus, some works targeted the development of US-MR registration methods, improving, therefore, the interpretability

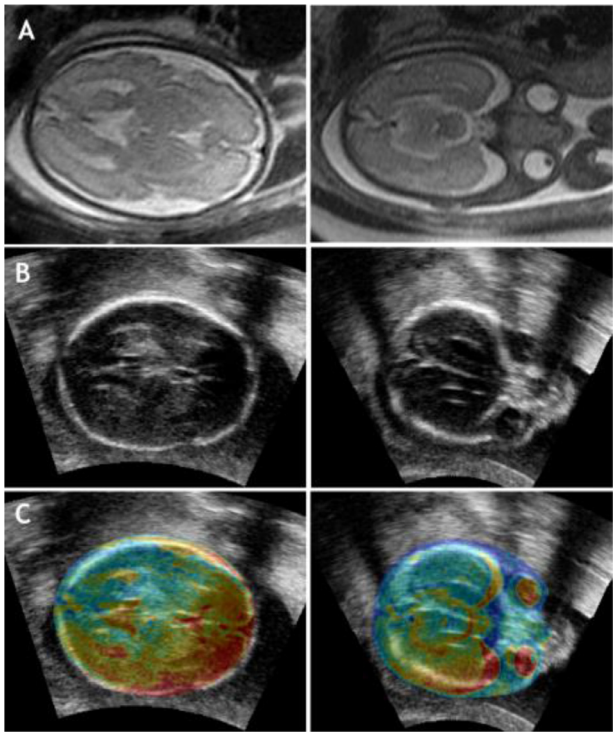

Fig. 12. Multimodal image registration of fetal head sequences. (A) MR images; (B) US images; (C) US image with MR information.

of US images thanks to the MR detail. In the work of Kuklisova-Murgasova et al. [133], the MR volume is firstly semi-automatically segmented using a probabilistic atlas, originating segmentation of brain and non-brain structures. Afterward, the segmentation image is converted to a US-like image where each region has an intensity assigned according to their expected echogenicity in a US image. The pseudo-US image is then registered with a real US image using a similarity measure and gradient descent optimization. The robustness of this method was later improved by introducing a robust block-matching algorithm for the alignment [134]. In [135], the segmentation of MR was fully automatized and registrations using gradient descent and block-matching algorithm were compared. In the work of Wright et al. [136], a DL strategy was proposed for the registration of 3D US and MR images. Here, a Long Short-Term Memory (LSTM) network inspired in the concept spatial transformer networks was used to simultaneously predict a joint isotropic rescaling and independent rigid transformations. Plus, transformation estimations are refined iteratively over time, improving the method's accuracy.

8.2. Performance assessment

The performance of the reviewed methods proposed for US image enhancement is shown in Table 11. One important aspect that should be noted is that direct evaluation metrics are difficult to implement for this type of methods. In [70], the alignment was evaluated by measuring the maximum distance inside the skull in estimated planes and the manual ones. Instead of using planes, a manual alignment of the volume was performed and the distance between a set of pairs of skull landmarks in the predicted aligned volume and the manually aligned volume are calculated in [126]. A similar approach was used to evaluate the registration methods, where registration errors are quantified by measuring the distance between a set of target points in the reference volume and the registered one [42,43,131,136]. Plus, the overlap between structures in the reference and registered image was also evalu-

Table 11
Performance assessment of image processing enhancement methods.

Reference	N	GA	Metric	Value
Cuingnet et al. [70]	78	19–24	ME_{TC}	5.8 mm
			ME_{TT}	5.1 mm
			ME_{TV}	5.3 mm
Namburete et al. [126]	140	22–30	ME	9.3 ± 4.4 mm
Perez-Gonzalez et al. [127]	10	20–24	SNR	10.53 ± 2.7
			CNR	12.13 ± 2.3
Cerrolaza et al. [129]	26	20–36	DSC, JI	80±4, 69±5%,
			AC, RE, SP	99±2, 91±4, 99±2%
Cerrolaza et al. [130]	14	20–36	DSC, RE, PR	91±2, 91±5, 91±6%
Perez-Gonzalez et al. [42]	7	20–24	ME	6.21 ± 3.78 mm
Perez-Gonzalez et al. [43]	18	20–24	ME	6.38 ± 3.24 mm
Fathima et al. [131]	30*	20	ME	3 ± 1 mm
Namburete et al. [132]	10*	23	RO	80.29 ± 4.9%
Murgasova et al. [134]	5*	28–29	ME	0.54 mm
Murgasova et al. [133]	27	18–22	RO	49.5 ± 10.8%
Murgasova et al. [135]	27	18–22	RO	51 ± 11%
Wright et al. [136]	166	20–21	ME	1.60 mm

AC: accuracy, DSC: Dice similarity coefficient, JI: Jaccard index, ME: mean error, PR: precision, RE: recall, RO: relative overlap, SP: specificity; *INTERGROWTH-21st data.

ated [132,134,135]. Concerning the compound methods, evaluation of SNR and contrast-to-noise (CNR) ratio was performed in [127]. In [129], skull occlusion was simulated to compare skull reconstruction with the expected skull volume.

8.3. Discussion

Besides reviewing image processing methods for head, brain, and standard planes analysis, this review also covered methods used to perform image enhancement of US images of the fetal head, including methods that find the head coordinate system, compounding approaches, and US and multimodal registration methods. As stated before, these types of approaches are useful to improve the information that can be retrieved from a US examination. Regarding compounding methods to fuse multi-view US volumes, statistical averaging or learning-based approaches are usually used to find the final image, usually after manual or semi-automatic image registration. Specifically, machine learning methods showed to be feasible to quantify the weight that each individual image must have in the final one. However, interestingly, the state-of-the-art learning-methods are mainly based on traditional machine learning techniques (e.g., SVM), not being verified the recent trend to replace this type of methods by DL-based approaches as verified for other image processing tasks, such as fetal segmentation/detection, anatomical plane analysis, or even for skull surface reconstruction reviewed in this section. Indeed, the compounding of US volumes of the fetal head/brain claims higher attention from the research field. Here, future research must be conducted to use DL approaches to create the final enhanced image, since DL strategies may have the ability to effectively and accurately learn how to maintain the importance features of the multiples views without overemphasizing the speckle noise or artifacts.

Concerning registration methods between US images, different measures of similarity were applied by the works. Moreover, two types of registrations were found, namely image-to-image registration and registration based on skull point clouds, proving both to be feasible. A more challenging task is the registration between US and MRI. When registering images from the same modality, the anatomical structures present similar intensity ranges, being possible to use image similarity to optimize the registration process. However, in multimodality image registration, the same anatomical structure may present different intensity values, precluding the use of traditional image similarity measures in the registration process. Here, intensity relationships between the modalities or handcrafted features (e.g., edges or mutual information) can be found and used as similarity metrics. However, establishing accurate metrics based on this information is difficult. Thus, in the literature for multimodal fetal head registration, early works adopted the strategy of transforming the MR image in an US-like image, using the information of segmented brain structures. This process enables the use of traditional image similarity measures, easing the registration using traditional optimization techniques. The drawback is that transforming a MR image into a US image still requires the usage of intensity relationships. Thus, more recent works for multimodal registration have been focused on the use of DL networks to find a similarity measure that represents the underlining correlation across modalities, also decreasing computational requirements in comparison with traditional registration. However, for the specific case of fetal images, this solution was not explored, mainly proposing DL approaches that directly predict image transformation parameters. Here, future improvements can be performed by adding information to the DL approach, such as the segmentation of some structures or even the use of similarity-based losses in combination with the transformation-based loss.

9. General current state of research and perspectives

Throughout the sections respecting to the five clinical applications described in this review, a discussion concerning the reviewed methods was performed. Here, the analysis of the proposed methods allowed to identify the most prominent techniques for each application, their advantages, and the current state of the research. A multitude of distinct image processing methods has been proposed for head and brain analysis in US, easing the evaluation of these anatomical structures, improving diagnosis stages, and therefore, providing more effective clinical routines. One of the major difficulties when comparing the methods was the fact that the databases used in the papers are very distinct, with a different number of images, different GA, and acquired with different acquisition parameters. This hampers the correct comparison between the reviewed methods. Moreover, due to the variable appearance of a US image depending on the acquisition settings (e.g., machine used, acquisition parameters, or operator experience), having an objective insight concerning the performance of the methods is complicated since image quality can vary significantly. Thus, the development of methods for quantitatively assessing the quality of a fetal US image can be helpful to retrieve accurate informa-

tion concerning the comparative performance of different methods. However, two challenges for fetal head analysis with public benchmarks were found in the literature. The *Challenge US: Biometric Measurements from Fetal Ultrasound Images* was a segmentation challenge that consisted of automatically segmenting anatomical structures, including the fetal head. The methods presented in this challenge were summarized in [137]. More recently, the *HC18 Challenge* [59] was developed to encourage the development of methods for fetal head circumference estimation in 2D ultrasound images, containing a dataset of training and testing images. Besides these challenges, several methods relied on the INTERGROWTH-21st project, which is an international study focused on acquiring fetal ultrasound image data and clinical biometrics [138]. As a remark, commercial software that includes image processing techniques to simplify fetal head/brain examination are already available, such as the 5D CNS+® from SAMSUNG, SmartPlanes® from Mindray, or SonoCNS from GE Voluson™.

Considering the analysis of the reviewed methods, it can be understood that despite different algorithmic approaches were proposed in the literature for fetal head/brain analysis, DL approaches seems to have been highly explored in the most recent years. In fact, it is possible to verify that these methods were useful for most tasks addressed in this review, and so, future improvements can be achieved using these types of methods. Here, besides the direct application of state-of-the-art networks, new architectures can be explored to boost the performance of methods (e.g., adding attention modules to the networks or including shape information). However, the application of such methods requires a strong database, which reinforces the need for public US benchmarks and for the development of approaches that deal with limited data (e.g., transfer learning approaches). Moreover, the computational cost associated with these methods is an important aspect once operation at time of acquisition can be foreseen. Thus, DL strategies with low complexity and cost should be analyzed for an efficient US evaluation.

From the authors' perspective, in the next years, it is needed an increase in the development of the methods for 3D shape analysis. In fact, 3D head segmentation will provide at least two major advantages. Firstly, it is well-known that 2D measurements provide rough estimations of the real 3D anatomical target, typically under/over-estimating the real value. Thus, potentiating 3D-based estimation of new volumetric biometrics, instead of the traditional bi-dimensional ones, can be useful to obtain a more accurate and realistic diagnosis. Secondly, 2D head segmentation does not allow creating an anatomical model representative of the fetal head, hampering the diagnose of certain abnormalities, such as cranial deformities. In this ambit, the creation of fetal head models can be achieved with a 3D delineation and subsequent shape analysis can be performed. The extraction of standard anatomical planes from a 3D volume is also a topic that is worthy to be more actively explored in the research field since the 3D imaging technology enabled data storage of the entire fetal head volume for offline analysis. Thus, automatic extraction of the standard 2D planes evaluated during the examination aids the evaluation of the stored data. Since 3D image acquisition is difficult, another application that it is worthy to be explored in the next years is the development of intelligent systems to optimize and even guide image acquisition [139].

Another application that should be explored in the next years is the automatic evaluation and quantification of certain fetal pathologies. No method was found in the literature to detect common fetal conditions, such as holoprosencephaly. Moreover, despite several methods were found for brain inner structures segmentation, no method was used or evaluated to segment abnormal structures. Furthermore, more effort should be made by the research community for the development of methods to detect lesions such as cysts or intracranial hemorrhage. This can bring added-value for the clinical practice to allow exact quantification of such lesions. Moreover, the evaluation of the proposed literature methods and future research methods in pathological cases should not be underestimated. Indeed, most of works assessed its performance in healthy cases. Nevertheless, the robustness of such methods in the presence of fetal pathologies is paramount to be used in clinical practice.

Finally, the development of image processing methods for fetal head and brain analysis is paramount for the monitoring of the fetus during the entire gestational period. However, as the head/brain develops during the fetal period, structural changes are verified. Thus, the development of a framework that enables the analysis throughout the pregnancy is not trivial. Indeed, most of the reviewed methods were proposed to address a specific gestational age range. Once more, DL approaches can present an advantage if a robust dataset that englobes all the gestational ages is used. However, prior knowledge about the gestational age can be used to increase the effectiveness of the methods and to provide a continuous quantitative analysis at the different evaluation stages. Thus, the development of advanced analytical tools for detailed fetal health status assessment will allow to continuously and accurately monitor neurodevelopment and head growth.

10. Conclusion

This work reviewed the methods related to the analysis of the head and brain in the context of fetal US. A multitude of image processing methods has been proposed for this analysis, mainly for five application areas: fetal head segmentation, brain inner structures analysis, standard anatomical planes identification, fetal developmental analysis, and image enhancement. For the five clinical applications studied, different types of theoretical approaches were explored, being the performance of each approach evaluated in terms of analysis success regarding its accuracy. Overall, different techniques proved their added-value for head and brain analysis, and therefore, for routine clinical practice.

Despite several methods were proposed for 2D US, the advances of image quality in 3D US allowed the emergence of approaches that explore 3D information. However, more effort should be made in the research area for the development of methods to segment the head in 3D images. Plus, methods to detect abnormalities or lesions in the fetal brain are also lacking in the literature. Finally, an effort must be made by the research community to use the same standardized metrics for the assessment of the segmentation/classification methods and more public benchmarks should be made available for all the researchers, allowing to boost this research topic and allowing a more reliable comparison between different approaches.

Declaration of Competing Interests

The authors declare that they have no known competing financial interests or personal relationships that could have appeared to influence the work reported in this paper.

CRediT authorship contribution statement

Helena R. Torres: Conceptualization, Methodology, Investigation, Writing – original draft. **Pedro Morais:** Methodology, Writing – review & editing. **Bruno Oliveira:** Methodology, Writing – review & editing. **Cahit Birdir:** Writing – review & editing. **Mario Rüdiger:** Writing – review & editing. **Jaime C. Fonseca:** Supervision, Funding acquisition, Writing – review & editing. **João L. Vilaça:** Supervision, Funding acquisition, Writing – review & editing.

Acknowledgments

This work was funded by projects "NORTE-01–0145-FEDER-000059", NORTE-01-0145-FEDER-024300 and "NORTE-01–0145-FEDER-000045", supported by Northern Portugal Regional Operational Programme (Norte2020), under the Portugal 2020 Partnership Agreement, through the European Regional Development Fund (FEDER). It was also funded by national funds, through the FCT – Fundação para a Ciência e Tecnologia within the R&D Units Project Scope: UIDB/00319/2020 and by FCT and FCT/MCTES in the scope of the projects UIDB/05549/2020 and UIDP/05549/2020. The authors also acknowledge support from FCT and the European Social Found, through Programa Operacional Capital Humano (POCH), in the scope of the PhD grant SFRH/BD/136670/2018 and SFRH/BD/136721/2018.

References

[1] S.L. Connors, et al., Fetal mechanisms in neurodevelopmental disorders, Pediatr. Neurol. 38 (3) (2008) 163–176.
[2] E. Merz, S. Pashaj, Advantages of 3D ultrasound in the assessment of fetal abnormalities, J. Perinat. Med. 45 (6) (2017) 643–650.
[3] A.S.L. Mak, K.Y. Leung, Prenatal ultrasonography of craniofacial abnormalities, Ultrasonography 38 (1) (2019) 13–24.
[4] B. Tutschek, et al., Three-dimensional ultrasound imaging of the fetal skull and face, Ultrasound Obstet. Gynecol. 50 (1) (2017) 7–16.
[5] G. Pilu, T. Ghi, A. Carletti, M. Segata, A. Perolo, N. Rizzo, Three-dimensional ultrasound examination of the fetal central nervous system, Ultrasound Obstet. Gynecol. 30 (2) (2007) 233–245.
[6] B. De Keersmaecker, F. Claus, L. De Catte, Imaging the fetal central nervous system, Facts Views Vis. ObGyn 3 (3) (2011) 135–149.
[7] J. Kurmanavicius, et al., Fetal ultrasound biometry–1. Head reference values, J. Obstet. Gynaecol. (Lahore). 106 (2) (1999) 126–135.
[8] K. Butt, et al., Determination of gestational age by ultrasound, J. Obstet. Gynaecol. Canada 36 (2) (2014) 171–181.
[9] A. Makropoulos, S.J. Counsell, D. Rueckert, A review on automatic fetal and neonatal brain MRI segmentation, Neuroimage 170 (2018) 231–248.
[10] O.M. Benkarim, et al., Toward the automatic quantification of in utero brain development in 3D structural MRI–A review, Hum. Brain Mapp. 38 (5) (2017) 2772–2787.
[11] J. Torrents-Barrena, et al., Segmentation and classification in MRI and US fetal imaging–Recent trends and future prospects, Med. Image Anal. 51 (2019) 61–88.
[12] H.R. Torres, S. Queirós, P. Morais, B. Oliveira, J.C. Fonseca, J.L. Vilaça, Kidney segmentation in ultrasound, magnetic resonance and computed tomography images–A systematic review, Comput. Methods Programs Biomed. 157 (Apr. 2018) 49–67.
[13] Z. Leibovitz, et al., Prediction of microcephaly at birth using three reference ranges for fetal head circumference–Can we improve prenatal diagnosis? Ultrasound Obstet. Gynecol. 47 (5) (2016) 586–592.
[14] A. Monteagudo, I.E. Timor-Tritsch, Ultrasound of the fetal brain, Ultrasound Clin. 2 (2) (2007) 217–244.
[15] D. Paladini, G. Malinger, A. Monteagudo, G. Pilu, I. Timor-Tritsch, A. Toi, Sonographic examination of the fetal central nervous system–Guidelines for performing the 'basic examination' and the 'fetal neurosonogram, Ultrasound Obstet. Gynecol. 29 (1) (2007) 109–116.
[16] G. Malinger, D. Paladini, K.K. Haratz, A. Monteagudo, G.L. Pilu, I.E. Timor-Tritsch, ISUOG practice guidelines (updated)–Sonographic examination of the fetal central nervous system. Part 1–Performance of screening examination and indications for targeted neurosonography, Ultrasound Obstet. Gynecol. 56 (3) (2020) 476–484.
[17] A.M. Coady, S. Bower, Twining's Textbook of Fetal Abnormalities, Churchill Livingstone, London, 2014.
[18] G. Pilu, Z. Alfirevic, "Fetal anomalies", in Fetal Medicine, B. Kumar and Z. Alfirevic, Eds. Cambridge University Press, 2016, pp. 81–95.
[19] M.J. Cornelissen, et al., Prenatal ultrasound parameters in single-suture craniosynostosis, J. Matern. Neonatal Med. 31 (15) (2018) 2050–2057.
[20] D. Paladini, P. Volpe, Ultrasound of Congenital Fetal Anomalies - Differential Diagnosis and Prognostic Indicators, 2nd ed., CRC Press Taylor & Francis, 2014.
[21] N.H. Khan, E. Tegnander, J.M. Dreier, S. Eik-Nes, H. Torp, G. Kiss, Automatic measurement of biparietal diameter with a portable ultrasound device, in: IEEE International Ultrasonics Symposium (IUS), 2014, pp. 459–462.
[22] H. Sahli, A. Zaafouri, A. Ben Slama, R. Rachdi, M. Sayadi, Analytic approach for fetal head biometric measurements based on log gabor features, Iran. J. Sci. Technol. Trans. A Sci. 43 (3) (2019) 1049–1057.
[23] C.F. Baumgartner, K. Kamnitsas, J. Matthew, S. Smith, B. Kainz, D. Rueckert, Real-time standard scan plane detection and localisation in fetal ultrasound using fully convolutional neural networks, in: International Conference on Medical Image Computing and Computer-Assisted Intervention, 2016, pp. 203–212.
[24] C.F. Baumgartner, et al., SonoNet–Real-time detection and localisation of fetal standard scan planes in freehand ultrasound, IEEE Trans. Med. Imaging 36 (11) (2017) 2204–2215.
[25] I.P. Satwika, M.I. Tawakal, Z. Imaduddin, W. Jatmiko, Efficient incomplete ellipse detection based on minor axis for ultrasound fetal head approximation, in: International Conference on Advanced Computer Science and Information Systems, 2012, pp. 191–195.
[26] I.P. Satwika, R. Rahmatullah, I. Habibie, A. Nurhadiyatna, W. Jatmiko, Improved efficient Ellipse Hough transform for fetal head measurement, in: International Conference on Advanced Computer Science and Information Systems (ICACSIS), 2013, pp. 375–379.
[27] I.P. Satwika, I. Habibie, M.A. Ma'Sum, A. Febrian, E. Budianto, Particle swarm optimation based 2-dimensional randomized hough transform for fetal head biometry detection and approximation in ultrasound imaging, in: International Conference on Advanced Computer Science and Information Systems (CACSIS), 2014, pp. 468–473.
[28] H. Sahli, A. Ben Slama, A. Zaafouri, M. Sayadi, R. Rachdi, Automated detection of current fetal head in ultrasound sequences, in: International Image Processing, Applications and Systems Conference, 2017, pp. 1–6.
[29] H. Sahli, A. Ben Slama, A. Mouelhi, N. Soayeh, R. Rachdi, M. Sayadi, A computer-aided method based on geometrical texture features for a precocious detection of fetal Hydrocephalus in ultrasound images, Technol. Health Care 1 (2020) 1–22.
[30] X. Liu, J. Yu, Y. Wang, P. Chen, Automatic localization of the fetal cerebellum on 3D ultrasound volumes, Med. Phys. 40 (11) (2013) 1–11.
[31] M.H. Marhaban, R.S. Kaid, S.B. Mohd Noor, Automatic estimation of gestational age in ultrasound images based on direct least-squares fitting of ellipse, IEEJ Trans. Electr. Electron. Eng. 5 (5) (2010) 569–573.
[32] M. Saii, Z. Kraitem, Determining the gestation age through the automated measurement of the bi-parietal distance in fetal ultrasound images, Ain Shams Eng. J. 9 (4) (2018) 2737–2743.
[33] G.V. Ponomarev, M.S. Gelfand, M.D. Kazanov, A multilevel thresholding combined with edge detection and shape-based recognition for segmentation of fetal ultrasound images, in: Proceedings of Challenge US–Biometric Measurements from Fetal Ultrasound Images ISBI, 2012, pp. 17–19.
[34] S.J. Sree, C. Vasanthanayaki, Texture-based fuzzy connectedness algorithm for fetal ultrasound image segmentation for biometric measurements, in: Soft Computing for Problem Solving, 2020, pp. 91–103.
[35] M.A. Ma'Sum, W. Jatmiko, M.I. Tawakal, F. Al Afif, Automatic fetal organs detection and approximation in ultrasound image using boosting classifier and hough transform, in: International Conference on Advanced Computer Science and Information Systems, 2014, pp. 460–467.
[36] W. Jatmiko, I. Habibie, M. Anwar Ma'sum, R. Rahmatullah, I.P. Satwika, Automated telehealth system for fetal growth detection and approximation of ultrasound images, Int. J. Smart Sens. Intell. Syst. 8 (1) (2015) 697–719.
[37] Z. Imaduddin, M.A. Akbar, H.A. Tawakal, I.P. Satwika, Y.B. Saroyo, Automatic detection and measurement of fetal biometrics to determine the Gestational Age, in: International Conference on Information and Communication Technology (ICoICT), 2015, pp. 608–612.
[38] E.A. Anto, B. Amoah, A. Crimi, Segmentation of ultrasound images of fetal anatomic structures using random forest for low-cost settings, in: IEEE Engineering in Medicine and Biology Society (EMBS), 2015, pp. 793–796.
[39] A.I.L. Namburete, J.A. Noble, Fetal cranial segmentation in 2D ultrasound images using shape properties of pixel clusters, in: International Symposium on Biomedical Imaging, 2013, pp. 720–723.
[40] R. Rahmatullah, M.A. Ma'Sum, P.Mursanto Aprinaldi, B. Wiweko, Automatic fetal organs segmentation using multilayer super pixel and image moment feature, in: International Conference on Advanced Computer Science and Information Systems, 2014, pp. 420–426.
[41] J.J. Cerrolaza, et al., Fetal skull segmentation in 3D ultrasound via structured geodesic random forest, in: Fetal, Infant and Ophthalmic Medical Image Analysis, 2017, pp. 25–32.
[42] J.L. Perez-Gonzalez, et al., Ultrasound fetal brain registration using weighted coherent point drift, International Symposium on Medical Information Processing and Analysis, 10160, 2017.
[43] J. Perez-Gonzalez, F. Arámbula Cosío, J.C. Huegel, V. Medina-Bañuelos, Probabilistic learning coherent point drift for 3D ultrasound fetal head registration, Comput. Math. Methods Med. 2020 (2020).
[44] T.L.A. Heuvel, H. Petros, S. Santini, C.L. de Korte, B. van Ginneken, Automated fetal head detection and circumference estimation from free-hand ultrasound sweeps using deep learning in resource-limited countries, Ultrasound Med. Biol. 45 (3) (2019) 773–785.
[45] O. Ronneberger, P. Fischer, T. Brox, "U-Net: Convolutional Networks for Biomedical Image Segmentation," in International Conference on Medical Image Computing and Computer-Assisted Intervention, 2015, pp. 234–241.
[46] H.P. Kim, S.M. Lee, J.Y. Kwon, Y. Park, K.C. Kim, J.K. Seo, Automatic evaluation of fetal head biometry from ultrasound images using machine learning, Physiol. Meas. 40 (6) (2019).
[47] J.J. Cerrolaza, et al., Deep learning with ultrasound physics for fetal skull segmentation, in: IEEE 15th International Symposium on Biomedical Imaging (ISBI), 2018, pp. 564–567.
[48] K.D. Rahayu, R. Sigit, D. Agata, Fetal head and femur detection from USG image to estimate gestational age, in: International Electronics Symposium on Knowledge Creation and Intelligent Computing, 2019, pp. 242–247.

[49] J. Banerjee, K.B. Krishnan, Model-based detection of acoustically dense objects in ultrasound, in: International Conference on Pattern Recognition (ICPR), 2010, pp. 4166–4169.
[50] D. Ni, et al., Learning based automatic head detection and measurement from fetal ultrasound images via prior knowledge and imaging parameters, in: Proceedings - International Symposium on Biomedical Imaging, 2013, pp. 772–775.
[51] J. Li, et al., Automatic fetal head circumference measurement in ultrasound using random forest and fast ellipse fitting, IEEE J. Biomed. Health Inform. 22 (1) (2018) 215–223.
[52] M. Yaqub, et al., Plane Localization in 3-D Fetal Neurosonography for Longitudinal Analysis of the Developing Brain, IEEE J. Biomed. Health Inform. 20 (4) (2016) 1–9.
[53] A. Foi, M. Maggioni, A. Pepe, J. Tohka, Head contour extraction from fetal ultrasound images by difference of Gaussians revolved along elliptical paths, in: Proceedings of Challenge US–Biometric Measurements from Fetal Ultrasound Images ISBI 2012, 2012, pp. 1–3. May.
[54] A. Foi, et al., Difference of Gaussians revolved along elliptical paths for ultrasound fetal head segmentation, Comput. Med. imaging Graph. 38 (8) (2014) 774–784.
[55] I. Kusuma, et al., Fetal head segmentation based on Gaussian elliptical path optimize by flower pollination algorithm and cuckoo search, in: International Conference on Advanced Computer Science and Information Systems (ICACSIS), 2017, pp. 564–571.
[56] M.A. Ma'Sum, N. Rahmah, H.R. Sanabila, H.A. Wisesa, W. Jatmiko, Automatic fetal head approximation using Particle Swarm Optimization based Gaussian Elliptical Path, International Symposium on Micro-NanoMechatronics and Human Science, 2016.
[57] R.V. Stebbing, J.E. McManigle, A boundary fragment model for head segmentation in fetal ultrasound, in: Proceedings of Challenge US–Biometric Measurements from Fetal Ultrasound Images, ISBI, 2012, pp. 9–11.
[58] L. Zhang, X. Ye, T. Lambrou, W. Duan, N. Allinson, N.J. Dudley, A supervised texton based approach for automatic segmentation and measurement of the fetal head and femur in 2D ultrasound images, Phys. Med. Biol. 61 (3) (2016) 1095–1115.
[59] T.L.A. Heuvel, D. de Bruijn, C.L. de Korte, B. van Ginneken, Automated measurement of fetal head circumference using 2D ultrasound images, PLoS ONE 4 (2018) 1–20.
[60] A. Ciurte, X. Bresson, M. Cuadra, A semi-supervised patchbased approach for segmentation of fetal ultrasound imaging, in: Proceedings of Challenge US–Biometric Measurements from Fetal Ultrasound Images ISBI, 2012, pp. 4–6. no. February.
[61] A. Ciurte, et al., Semi-supervised segmentation of ultrasound images based on patch representation and continuous min cut, PLoS ONE 9 (7) (2014).
[62] C. Sun, Automatic fetal head measurements from ultrasound images using circular shortest paths, in: Proceedings of Challenge US–Biometric Measurements from Fetal Ultrasound Images ISBI, 2012, pp. 13–14.
[63] H.C. Chen, et al., Registration-based segmentation of three-dimensional ultrasound images for quantitative measurement of fetal craniofacial structure, Ultrasound Med. Biol. 38 (5) (2012) 811–823.
[64] J.L. Perez-Gonzalez, J.B. Muńoz, M.R. Porras, F. Arámbula-Cosío, V. Medina-Bańuelos, Automatic fetal head measurements from ultrasound images using optimal ellipse detection and texture maps, in: Latin American Congress on Biomedical Engineering CLAIB, 2014, pp. 329–332.
[65] V. Rawat, A. Jain, V. Shrimali, A. Rawat, Automatic detection of fetal abnormality using head and abdominal circumference, in: International Conference on Computational Collective Intelligence, 2016, pp. 525–534.
[66] Y. Rong, et al., Deriving external forces via convolutional neural networks for biomedical image segmentation, Biomed. Opt. Express 10 (8) (2019) 3800.
[67] A.V. Gadagkar, K.S. Shreedhara, Features based IUGR diagnosis using variational level set method and classification using artificial neural networks, in: International Conference on Signal and Image Processing (ICSIP), 2014, pp. 303–309.
[68] V. Rajinikanth, N. Dey, R. Kumar, J. Panneerselvam, N. Sri Madhava Raja, Fetal head periphery extraction from ultrasound image using jaya algorithm and Chan-Vese segmentation, Procedia Comput. Sci. 152 (2019) 66–73.
[69] A.I.L. Namburete, R.V. Stebbing, J.A. Noble, Cranial parametrization of the fetal head for 3D ultrasound image analysis, in: Medical Image Understanding and Analysis (MIUA), 2013, pp. 196–201.
[70] R. Cuingnet, et al., Where is my baby? A fast fetal head auto-alignment in 3D-ultrasound, in: International Symposium on Biomedical Imaging (ISBI), 2013, pp. 768–771.
[71] L. Wu, Y. Xin, S. Li, T. Wang, P.A. Heng, D. Ni, Cascaded Fully Convolutional Networks for automatic prenatal ultrasound image segmentation, in: International Symposium on Biomedical Imaging (ISBI), 2017, pp. 663–666.
[72] M. Sinclair, et al., Human-level Performance on automatic head biometrics in fetal ultrasound using fully convolutional neural networks, IEEE Eng. Med. Biol. Soc. (EMBS) (2018) 714–717 2018-July.
[73] M. Yaqub, B. Kelly, A.T. Papageorghiou, J.A. Noble, A deep learning solution for automatic fetal neurosonographic diagnostic plane verification using clinical standard constraints, Ultrasound Med. Biol. 43 (12) (2017) 2925–2933.
[74] H. Xie, et al., Using deep learning algorithms to classify fetal brain ultrasound images as normal or abnormal, Ultrasound Obstet. Gynecol. 56 (4) (2020) 579–587.
[75] B. Al-Bander, T. Alzahrani, S. Alzahrani, B.M. Williams, Y. Zheng, Improving fetal head contour detection by object localization with deep learning, in: Annual Conference on Medical Image Understanding and Analysis, 2019, pp. 142–150.
[76] A. Chaurasia, E. Culurciello, LinkNet–Exploiting encoder representations for efficient semantic segmentation, in: 2017 IEEE Visual Communications and Image Processing (VCIP), 2018-January, 2018, pp. 1–4.
[77] Z. Sobhaninia, et al., Fetal ultrasound image segmentation for measuring biometric parameters using multi-task deep learning, in: IEEE Engineering in Medicine and Biology Society (EMBC), 2019, pp. 6545–6548.
[78] Z. Sobhaninia, A. Emami, N. Karimi, S. Samavi, Localization of fetal head in ultrasound images by multiscale view and deep neural networks, in: International Computer Conference, Computer Society of Iran, CSICC, 2020, 2020, pp. 1–5.
[79] R. Huang, W. Xie, J.A. Noble, VP-Nets efficient automatic localization of key brain structures in 3D fetal neurosonography, Med. Image Anal. 47 (2018) 127–139.
[80] H. Ye, K. Feng, L. Luo, and H. Xie, "Ultrasonic image segmentation method based on improved fully convolution network," vol. 87, no. Icmeit, pp. 581–584, 2019.
[81] S. Budd, et al., Confident head circumference measurement from ultrasound with real-time feedback for sonographers, in: Lecture Notes in Computer Science (including subseries Lecture Notes in Artificial Intelligence and Lecture Notes in Bioinformatics), 11767, 2019, pp. 683–691. LNCS.
[82] F. Moser, R. Huang, A.T. Papageorghiou, B.W. Papież, A.I.L. Namburete, Automated fetal brain extraction from clinical ultrasound volumes using 3D convolutional neural networks, in: Communications in Computer and Information Science, 1065, 2020, pp. 151–163. CCIS.
[83] X. Yang, et al., Hybrid attention for automatic segmentation of whole fetal head in prenatal ultrasound volumes, Comput. Methods Programs Biomed. 194 (April) (2020) 105519.
[84] P. Liu, H. Zhao, P. Li, F. Cao, Automated classification and measurement of fetal ultrasound images with attention feature pyramid network, Second Target Recognition and Artificial Intelligence Summit Forum, 2020.
[85] Y. Zhang, J. Gao, H. Zhou, ImageNet classification with deep convolutional neural networks alex, Adv. Neural Inf. Process. Syst. 25 (2012) 1097–1105.
[86] M. Yaqub, R. Napolitano, C. Ioannou, A.T. Papageorghiou, J.A. Noble, Automatic detection of local fetal brain structures in ultrasound images, in: IEEE International Symposium on Biomedical Imaging (ISBI), 2012, pp. 1555–1558.
[87] Y. Li, et al., Fast multiple landmark localisation using a patch-based iterative network, in: International Conference on Medical Image Computing and Computer-Assisted Intervention, 2018, pp. 563–571.
[88] A. Alansary, et al., Evaluating reinforcement learning agents for anatomical landmark detection, Med. Image Anal. 53 (2019) 156–164.
[89] M. Sofka, K. Ralovich, N. Birkbeck, J. Zhang, S.K. Zhou, Integrated Detection Network (IDN) for pose and boundary estimation in medical images, in: International Symposium on Biomedical Imaging, 2011, pp. 294–299.
[90] M. Sofka, J. Zhang, S. Good, S.K. Zhou, D. Comaniciu, Automatic detection and measurement of structures in fetal head ultrasound volumes using sequential estimation and integrated detection network (IDN), IEEE Trans. Med. Imaging 33 (5) (2014) 1054–1070.
[91] H. Luo, H. Liu, K. Li, B. Zhang, Automatic quality assessment for 2D fetal sonographic standard plane based on multi-task learning, Med. Image Anal. (2019).
[92] Z. Lin, et al., Quality assessment of fetal head ultrasound images based on faster R-CNN, in: Simulation, Image Processing, and Ultrasound Systems for Assisted Diagnosis and Navigation, 1, 2018, pp. 38–46.
[93] Z. Lin, et al., Multi-task learning for quality assessment of fetal head ultrasound images, Med. Image Anal. 58 (2019) 101548.
[94] R. Ramos, J. Olveres, B. Escalante-Ramírez, F. Arambula, Deep learning approach for cerebellum localization in prenatal ultrasound images, Optics, Photonics and Digital Technologies for Imaging Applications VI, 11353, 2020.
[95] P. Annangi, K. Banerjee Krishnan, J. Banerjee, M. Gupta, U. Patil, Automatic detection and estimation of biparietal diameter from fetal ultrasonography, in: Medical Imaging 2011–Ultrasonic Imaging, Tomography, and Therapy, 7968, 2011, p. 79680I.
[96] P. Sridar, et al., Automatic measurement of thalamic diameter in 2D fetal ultrasound brain images using shape prior constrained regularized level sets, IEEE J. Biomed. Health Inform. 21 (4) (2017) 1069–1078.
[97] W. Lu, J. Tan, R. Floyd, Automated fetal head detection and measurement in ultrasound images by iterative randomized hough transform, Ultrasound Med. Biol. 31 (7) (2005) 929–936.
[98] I. Waechter-Stehle, et al., Learning from redundant but inconsistent reference data–Anatomical views and measurements for fetal brain screening, in: Medical Imaging–Image Processing, 9784, 2016, p. 97841A.
[99] B. Gutiérrez-Becker, F. Arambula Cosio, M.E. Guzman Huerta, J.A. Benavides-Serralde, Automatic segmentation of the cerebellum of fetuses on 3D ultrasound images, using a 3D Point Distribution Model, in: IEEE Engineering in Medicine and Biology Society, 2010, pp. 4731–4734.
[100] B. Gutiérrez-Becker, F. Arámbula Cosío, M.E. Guzmán Huerta, J.A. Benavides-Serralde, L. Camargo-Marín, V. Medina Bañuelos, Automatic segmentation of the fetal cerebellum on ultrasound volumes, using a 3D statistical shape model, Med. Biol. Eng. Comput. 51 (9) (2013) 1021–1030.
[101] G. Velásquez-Rodríguez, F. Arámbula, M. Guzmán, L. Camargo, H. Borboa, Automatic segmentation of the cerebellum in ultrasound volumes of the fetal brain, Rev. Mex. Ing. Bioméd. 36 (2) (2015) 121–129.
[102] G. Velásquez-Rodríguez, F.Arámbula Cosío, B.Escalate Ramírez, Automatic segmentation of the fetal cerebellum using spherical harmonics and gray level

profiles, International Symposium on Medical Information Processing and Analysis, 9681, 2015.
[103] M.R. López, F.A. Cosío, Statistical shape (ASM) and appearance (AAM) models for the segmentation of the cerebellum in fetal ultrasound, International Conference on Medical Information Processing and Analysis, 10572, 2017.
[104] M.R. López, F.A. Cosío, B. Escalante-Ramírez, J. Olveres, Shape model and Hermite features for the segmentation of the cerebellum in fetal ultrasound, International Symposium on Medical Information Processing and Analysis, 10975, 2018.
[105] M. Yaqub, et al., Volumetric segmentation of key fetal brain structures in 3D ultrasound, in: International Workshop on Machine Learning in Medical Imaging, 8184, 2013, pp. 25–32. LNCS.
[106] R. Huang, A.I.L. Namburete, A. Noble, Learning to segment key clinical anatomical structures in fetal neurosonography informed by a region-based descriptor, J. Med. Imaging 5 (01) (2018) 1.
[107] L. Venturini, A.T. Papageorghiou, J.A. Noble, A.I.L. Namburete, Multi-task CNN for Structural Semantic Segmentation in 3D Fetal Brain Ultrasound, in: Annual Conference on Medical Image Understanding and Analysis, 2019, pp. 164–173.
[108] F. Milletari, N. Navab, S.A. Ahmadi, V-Net–Fully convolutional neural networks for volumetric medical image segmentation, in: Proceedings - 2016 4th International Conference on 3D Vision, 3DV 2016, 2016, pp. 565–571.
[109] M.A. Maraci, et al., Toward point-of-care ultrasound estimation of fetal gestational age from the trans-cerebellar diameter using CNN-based ultrasound image analysis, J. Med. Imaging 7 (01) (2020) 1.
[110] A.I.L. Namburete, R. Stebbing, J. Noble, Diagnostic plane extraction from 3D parametric surface of the fetal cranium, in: Medical Image Understanding and Analysis (MIUA), 2014, pp. 27–32.
[111] eter M. Yaqub, A. Kopuri, S. RuedaP, B. Sullivan, K. McCormick, J.A. Noble, A constrained regression forests solution to 3D fetal ultrasound plane localization for longitudinal analysis of brain growth and maturation, in: International Workshop on Machine Learning in Medical Imaging, 8679, 2014, pp. 109–116.
[112] Y. Li, et al., Standard plane localisation in 3D fetal ultrasound using network with geometric and image loss, in: Medical Imaging with Deep Learning (MIDP), 2018, pp. 3–5.
[113] Y. Li, et al., Standard plane detection in 3D fetal ultrasound using an iterative transformation network, in: International Conference on Medical Image Computing and Computer-Assisted Intervention, 2018, pp. 392–400.
[114] L.J. Salomon, J.P. Bernard, M. Duyme, B. Doris, N. Mas, Y. Ville, Feasibility and reproducibility of an image-scoring method for quality control of fetal biometry in the second trimester, Ultrasound Obstet. Gynecol. 27 (1) (2006) 34–40.
[115] L. Zhang, N.J. Dudley, T. Lambrou, N. Allinson, X. Ye, Automatic image quality assessment and measurement of fetal head in two-dimensional ultrasound image, J. Med. Imaging 4 (2) (2017) 024001.
[116] M. Yaqub, B. Kelly, A.T. Papageorghiou, J.A. Noble, Guided random forests for identification of key fetal anatomy and image categorization in ultrasound scans, in: Medical Image Computing and Computer-Assisted Intervention, 9351, 2015, pp. 12–20.
[117] X. Liu, et al., Learning-based scan plane identification from fetal head ultrasound images, in: Medical Imaging 2012–Ultrasonic Imaging, Tomography, and Therapy, 8320, 2012, p. 83200A.
[118] R. Qu, G. Xu, C. Ding, W. Jia, M. Sun, Deep learning-based methodology for recognition of fetal brain standard scan planes in 2D ultrasound images, IEEE Access 8 (2020) 44443–44451.
[119] R. Qu, G. Xu, C. Ding, W. Jia, M. Sun, Standard plane identification in fetal brain ultrasound scans using a differential convolutional neural network, IEEE Access (2020) 83821–83830.
[120] J. Schlemper et al., "Attention-gated networks for improving ultrasound scan plane detection," in arXiv preprint, 2018, pp. 1–12.
[121] A.I.L. Namburete, M. Yaqub, B. Kemp, A.T. Papageorghiou, J.A. Noble, Predicting fetal neurodevelopmental age from ultrasound images, in: International conference on medical image computing and computer-assisted intervention, 2014, pp. 260–267.
[122] A.I.L. Namburete, R.V. Stebbing, B. Kemp, M. Yaqub, A.T. Papageorghiou, J.Alison Noble, Learning-based prediction of gestational age from ultrasound images of the fetal brain, Med. Image Anal. 21 (1) (2015) 72–86.
[123] H. Sahli, A. Mouelhi, A. Ben Slama, M. Sayadi, R. Rachdi, Supervised classification approach of biometric measures for automatic fetal defect screening in head ultrasound images, J. Med. Eng. Technol. 43 (5) (2019) 279–286.
[124] H. Sahli, A. Mouelhi, M. Sayadi, R. Rachdi, Discriminant textural feature selection and classification for a computerized fetal hydrocephalus detection, in: International Conference on Image Processing, Applications and Systems, 2018, pp. 232–237.
[125] F.P. Hadlock, R.B. Harrist, R.S. Sharman, R.L. Deter, S.K. Park, Estimation of fetal weight with the use of head, body, and femur measurements–A prospective study, Am. J. Obstet. Gynecol. 151 (3) (1985) 333–337.
[126] A.I.L. Namburete, W. Xie, M. Yaqub, A. Zisserman, J.A. Noble, Fully-automated alignment of 3D fetal brain ultrasound to a canonical reference space using multi-task learning, Med. Image Anal. 46 (2018) 1–14.
[127] J. Perez-Gonzalez, et al., Spatial compounding of 3D fetal brain ultrasound using probabilistic maps, Ultrasound Med. Biol. 44 (1) (2018) 278–291.
[128] R. Wright, et al., Complete fetal head compounding from multi-view 3D ultrasound, in: International Conference on Medical Image Computing and Computer-Assisted Intervention, 2019, pp. 384–392.
[129] J.J. Cerrolaza, et al., Fetal skull reconstruction via deep convolutional autoencoders, in: Proceedings of the Annual International Conference of the IEEE Engineering in Medicine and Biology Society, 2018-July, EMBS, 2018, pp. 887–890.
[130] J.J. Cerrolaza, et al., 3D fetal skull reconstruction from 2DUS via deep conditional generative networks, in: International Conference on Medical Image Computing and Computer-Assisted Intervention, 57, 2018, pp. 59–67.
[131] S. Fathima, S. Rueda, A. Papageorghiou, J.A. Noble, A novel local-phase method of automatic atlas construction in fetal ultrasound, in: Medical Imaging 2011–Image Processing, 7962, 2011, p. 79621A.
[132] A.I.L. Namburete, R. van Kampen, A.T. Papageorghiou, B.W. Papiez, Multi-channel groupwise registration to construct an ultrasound-specific fetal brain atlas, in: Data Driven Treatment Response Assessment and Preterm, Perinatal, and Paediatric Image Analysis, 1, 2018, pp. 76–86.
[133] M. Kuklisova-Murgasova, G. Quaghebeur, J.V. Hajnal, J.A. Noble, J.A. Schnabel, Towards 3D registration of fetal brain MRI and ultrasound, in: Proceedings IEEE International Symposium on Biomedical Imaging, 2012, pp. 346–349.
[134] M. Kuklisova-Murgasova, et al., Registration of 3D fetal brain US and MRI, in: International Conference on Medical Image Computing and Computer-Assisted Intervention, 2012, pp. 667–674.
[135] M. Kuklisova-Murgasova, et al., Registration of 3D fetal neurosonography and MRI, Med. Image Anal. 17 (8) (2013) 1137–1150.
[136] R. Wright, et al., LSTM spatial co-transformer networks for registration of 3D fetal US and MR brain images, in: Driven Treatment Response Assessment and Preterm, Perinatal, and Paediatric Image Analysis, 1, 2018, pp. 149–159.
[137] S. Rueda, et al., Evaluation and comparison of current fetal ultrasound image segmentation methods for biometric measurements–A grand challenge, IEEE Trans. Med. Imaging 33 (4) (2014) 797–813.
[138] A.T. Papageorghiou, et al., International standards for fetal growth based on serial ultrasound measurements–The fetal growth longitudinal study of the INTERGROWTH-21st project, Lancet 384 (9946) (2014) 869–879.
[139] L. Drukker, J.A. Noble, A.T. Papageorghiou, Introduction to artificial intelligence in ultrasound imaging in obstetrics and gynecology, Ultrasound Obstet. Gynecol. 56 (4) (2020) 498–505.
[140] P. Nadiyah, N. Rofiqah, Q. Firdaus, R. Sigit, H. Yuniarti, Automatic detection of fetal head using Haar Cascade and Fit Ellipse, in: Proceedings - 2019 International Seminar on Intelligent Technology and Its Application, ISITIA 2019, 2019, pp. 320–324.